REVIEW ON NEUTRINO OSCILLATIONS*

André Rubbia

Institut für Teilchenphysik, ETHZ
CH-8093 Zürich, Switzerland
e-mail: andre.rubbia@cern.ch

(Received April 30, 1999)

This article summarizes the current status of neutrino oscillations. After briefly recalling the theoretical framework of neutrino masses and mixing, we describe in more details the experimental situation. The current three experimental hints for oscillations are summarized. We discuss in some details the negative searches for $\nu_\mu \to \nu_\tau$ oscillations at high Δm^2. Then, the effects seen in LSND and in the solar and atmospheric neutrinos that could all be explained in terms of neutrino oscillations are described. We also address with a brief overview on the future possibilities, in particular the long baseline programmes, the solutions that will help clarify and possibly confirm or disprove the current observed effects.

PACS numbers: 13.15.+g, 14.60.Lm, 14.60.Pq, 14.60.St

1. Introduction

1.1. Theoretical overview

The theoretical perspective concerning neutrino masses has changed considerably over the past 20 years. Before that time, there was no theoretical reason for neutrinos to have masses, which was in accord with the striking fact that the upper limits on their masses were much smaller than those of the associated charged leptons. The experimental data was also suggesting the conservation "laws" of lepton family number and total lepton number.

Today, there are still no firm theoretical predictions for neutrino masses or mixing matrices but several experimental hints have been accumulated over the years that could indicate that neutrinos are indeed massive and exhibit the phenomenon of flavor oscillation [1]. This has led to a search for natural extension of the Standard Model which could include massive

* Presented at the XXVII International Meeting on Fundamental Physics, Sierra Nevada, Granada, Spain, February 1–5, 1999.

neutrinos. The possibility to consider neutrinos as massive objects opens ways to new static properties such as flavor mixing and oscillations, magnetic moments, decays, *etc.*

1.2. Dirac and Majorana neutrinos

Let us recall the basic theoretical description of the neutrinos. The three neutrinos ν_e, ν_μ and ν_τ are defined as the weak isopartners of the charged leptons:

$$\begin{pmatrix} \nu_{e\mathrm{L}} \\ e_{\mathrm{L}} \end{pmatrix}; \begin{pmatrix} \nu_{\mu\mathrm{L}} \\ \mu_{\mathrm{L}} \end{pmatrix}; \begin{pmatrix} \nu_{\tau\mathrm{L}} \\ \tau_{\mathrm{L}} \end{pmatrix}; e_{\mathrm{R}}; \mu_{\mathrm{R}}; \tau_{\mathrm{R}}\,. \tag{1}$$

With this particle assignment, the electron gets a Dirac mass

$$m_e(\bar{e}_{\mathrm{L}} e_{\mathrm{R}} + \mathrm{h.c.}). \tag{2}$$

In the Standard Model, only one helicity state of the neutrino per generation is present. Therefore, it could not have a Dirac mass, which requires both helicity states. If neutrinos are massive, it is tempting to think that they are like any other fermions, *i.e.* described by a Dirac spinor. In presence of the right handed field, a natural mass term is:

$$-\mathcal{L}_{\mathrm{Dirac}} = m_D \bar{\nu}_{\mathrm{L}} \nu_{\mathrm{R}} + \mathrm{h.c.} \qquad (|\Delta L| = 0)\,, \tag{3}$$

where ν_{R} are the right-handed neutrino singlets ($Y = 0$). This mass term conserves lepton number since it involves an incoming right handed and an outgoing left handed neutrino. All experiments to date are consistent with the neutrino being left handed (ν_{L}) and the anti-neutrino being right handed (ν^c_{R}). Whether the two other states ν_{R} and ν^c_{L} exist in Nature (in analogy to the electron states) is at present unknown. In the Dirac neutrino scenario, the mass term for the neutrinos can be generated by the vacuum expectation value (*vev*) as for the other fermions.

An alternative type of mass terms, called Majorana mass terms, could then be possible even without additional right-handed neutrinos. It requires just one helicity state of the particle and uses the opposite helicity state of the antiparticle. The mass generation therefore involves a transition from an antineutrino into a neutrino, *i.e.* $|\Delta L| = 2$. This mass term violates lepton number by two units, which is incompatible with the principles of the Standard Model which conserves the quantum number $B - L$. A Majorana mass term will be of the form:

$$-\mathcal{L}_{\mathrm{Majorana}} = m_{\mathrm{L}} \bar{\nu}_{\mathrm{L}} \nu^c_{\mathrm{R}} + \mathrm{h.c.} \qquad (|\Delta L| = 2)\,. \tag{4}$$

In the Majorana neutrino scenario, lepton number is a global symmetry and spontaneously broken via the vacuum expectation value of an $I = 1$

complex scalar field. The coupling of the neutral field to neutrinos give the left-handed $\nu's$ a Majorana mass ($m_{\rm L}$). The massless Goldstone field is called the Majoron. The masses m_ν remain arbitrary. One can also consider the $I = 1$ complex field as a way of expressing a product of two $I = \frac{1}{2}$ "standard" Higgs multiplets.

In general, we can have also a "right-handed-type" Majorana mass term of the form:

$$-{\rm L}_{\rm Majorana} = m_{\rm R}\bar{\nu}^c_{\rm L}\nu_{\rm R} + {\rm h.c.} \qquad (|\Delta L| = 2)\,. \tag{5}$$

The right-handed states $\nu_{\rm R}$ do not need to be the "partners" of the ordinary neutrino. They can be other heavier states which can mix with ordinary neutrinos.

A general neutrino mass term can involve both Dirac and Majorana mass terms. In this case, one can write the mass term in the following way:

$$-\mathcal{L}_{\rm mixed} = \frac{1}{2}\,(\bar{\nu}_{\rm L}\bar{\nu}^c_{\rm L}) \begin{pmatrix} m_{\rm L} & m_D \\ m_D & m_{\rm R} \end{pmatrix} \begin{pmatrix} \nu^c_{\rm R} & \nu_{\rm R} \end{pmatrix}, \tag{6}$$

where $m_{\rm L}$ and $m_{\rm R}$ are Majorana mass terms and m_D is a Dirac mass term. The physical particle content is given by two Majorana mass eigenstates:

$$m_{1,2} = \frac{1}{2}\left[(m_{\rm L} + m_{\rm R}) \pm \sqrt{(m_{\rm L} - m_{\rm R})^2 + 4m_D^2}\right]. \tag{7}$$

In the limit where $m_{\rm R} = m_{\rm L} = 0$, the two Majorana mass eigenstates are degenerate and can be combined to form a Dirac neutrino.

An especially interesting case is the see-saw limit, where $m_{\rm L} = 0$ and $m_D \ll m_{\rm R}$, in which there are two Majorana neutrinos with masses:

$$m_1 \approx m_{\rm R}; \tag{8}$$

$$m_2 \approx \frac{m_D^2}{m_{\rm R}} \ll m_D\,, \tag{9}$$

where m_D is assumed to be of the order of the quark and charged lepton masses, and $m_{\rm R}$ is a large mass of the order of some unification scale. This forces the mass of the neutrino to be small, and postulates a very heavy right-handed neutrino, therefore decoupling it from interactions in the accessible energy range. Thus, the see-saw mechanism is a popular way of generating light ordinary neutrino masses.

1.3. Sterile neutrinos

For an ordinary Dirac neutrino, the $\nu_{\rm L}$ belonging to the ${\rm SU(2)_L}$ doublet is active and the $\nu_{\rm R}$ being the ${\rm SU(2)_L}$ singlet does not exhibit weak interactions except those due to mixing and is therefore called *sterile*. Recently,

an approach to study sterile neutrinos as light particle, which disagrees with the canonical view of the singlet states being very heavy, has been revived. Although all the masses of all neutral singlet states are arbitrary and independent, it can be considered as natural to expect them to be of some scale of the theory. The lightness of the ordinary neutrinos, however, gives already evidence that very disparate mass scales can coexist in Nature and we can therefore assume the sterile neutrinos to be light for the similar reasons that make the ordinary doublet neutrinos light.

1.4. Neutrino masses

Neutrino mass phenomenology is more complicated than the one of the charged leptons. The neutrino has no electric charge and this opens new possibilities for mechanisms generating its mass. The question of whether Majorana mass terms are allowed or forbidden will depend on whether Nature has produced a Higgs field which can break lepton number by two units. Since other fermions are charged, such transitions are forbidden by charge conservation and therefore neutrinos would have a really priviledged situation.

The current experimental limits on direct kinematical searches for neutrino masses are shown in Table I.

TABLE I

Direct neutrino mass measurements from kinematic distributions of weak decays

Neutrino Type	Mass Limit	Process
Electron	$<\sim 10$ eV	${}^3H \to {}^3He + e^- + \nu_e$
Muon	< 170 keV	$\pi^+ \to \mu^+ + \nu_\mu$
Tau	< 18.2 MeV	$\tau \to 5\pi\,(\pi^0) + \nu_\tau$

1.5. Neutrino flavor oscillations

If neutrino are massive, it is likely that the mass eigenstates do not exactly coincide with the weak eigenstates. In this case, considering for simplicity the case of two neutrinos, the weak eigenstates can be written as linear combinations of the mass eigenstates:

$$\begin{pmatrix} \nu_e \\ \nu_\mu \end{pmatrix} = \begin{pmatrix} \cos\theta & \sin\theta \\ -\sin\theta & \cos\theta \end{pmatrix} \begin{pmatrix} \nu_1 \\ \nu_2 \end{pmatrix}, \tag{10}$$

where θ is the mixing angle. In this case, a pure weak eigenstates ν_α will be the sum of two mass eigenstates that will propagate with different phases in

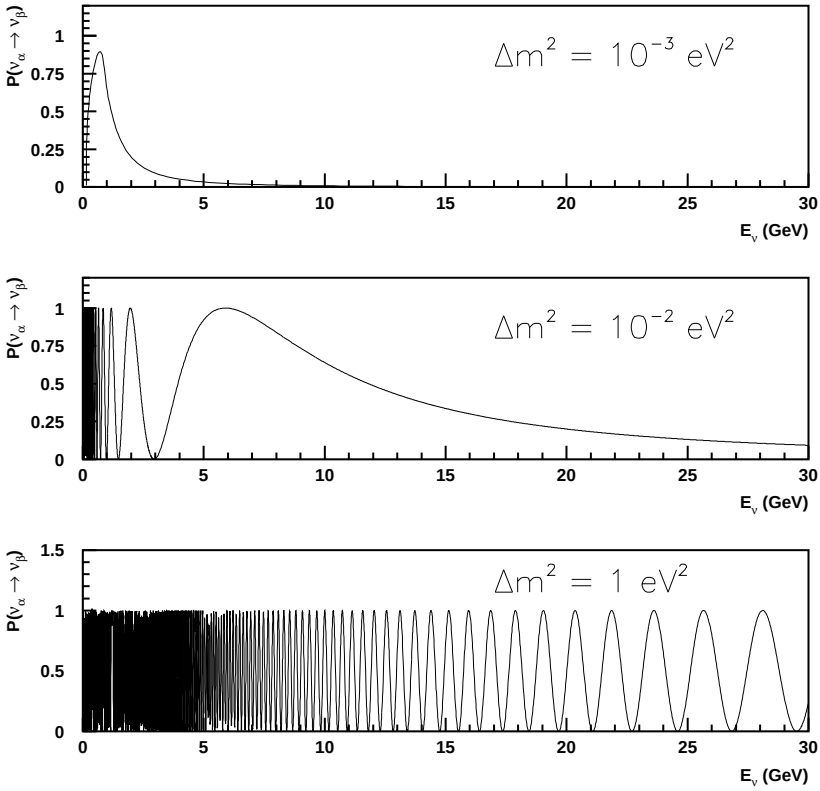

Fig. 1. Oscillation probability as a function of neutrino energy for a baseline of 730 km for (a) $\Delta m^2 = 10^{-3}$ eV^2 (b) $\Delta m^2 = 10^{-2}$ eV^2 (c) $\Delta m^2 = 1$ eV^2.

space if their masses are different. At a given distance from the source L, there will be probability

$$P(\nu_\alpha \to \nu_\beta) = \sin^2 2\theta \sin\left(1.27\Delta \mathrm{m}^2(\mathrm{eV}^2)\frac{L(\mathrm{km})}{E(\mathrm{GeV})}\right)$$

to observe a neutrino of a different flavor ν_β ($\alpha \neq \beta$). This oscillatory behavior is illustrated in figure 1 as a function of the neutrino energy.

The charged current transitions involve a leptonic mixing matrix which in the most general case includes oscillations between all three neutrino

species. This can be expressed as:

$$\begin{pmatrix} \nu_e \\ \nu_\mu \\ \nu_\tau \end{pmatrix} = \begin{pmatrix} U_{e1} & U_{e2} & U_{e3} \\ U_{\mu 1} & U_{\mu 2} & U_{\mu 3} \\ U_{\tau 1} & U_{\tau 2} & U_{\tau 3} \end{pmatrix} \begin{pmatrix} \nu_1 \\ \nu_2 \\ \nu_3 \end{pmatrix} .$$

This formalism is analogous to the quark sector, where mass and weak eigenstates are not identical and the resultant mixing is described conventionally by a unitary mixing matrix. Up to now, one has ignored possible CP violation, then U is real. The oscillation probability is then:

$$P\left(\nu_\alpha \to \nu_\beta\right) = \delta_{\alpha\beta} - 4 \sum_{j>i} U_{\alpha i} U_{\beta i} U^*_{\alpha j} U^*_{\beta j} \sin^2 \left(\frac{1.27 \Delta m^2_{ij} L}{E} \right) , \qquad (11)$$

where $\Delta m^2_{ij} = \left| m^2_i - m^2_j \right|$.

With three neutrinos, there are two independent mass differences, say Δm^2_{21} and Δm^2_{32}, since $\Delta m^2_{21} + \Delta m^2_{32} = \Delta m^2_{31}$ and three different mixing angles.

Although in general there will be mixing among all three flavors of neutrinos, two-generation mixing is often assumed for simplicity. Assuming a hierarchy like the one in the quark sector, the condition $m_1 \ll m_2 \ll m_3$ implies

$$\Delta m^2_{21} < \Delta m^2_{31} \approx \Delta m^2_{32}, \qquad (12)$$

with two light almost degenerate neutrinos and one heavier one[1].

Then, oscillation phenomena tend to decouple and the two-generation mixing model is a good approximation in limited regions. In this case, each transition can be described by a two-generation mixing equation, with two kinds of oscillations, one "short" and one "long". The transitions $\nu_\mu \to \nu_e$ and $\nu_\mu \to \nu_\tau$ occur with the following probabilities:

$$P_{\text{short}}(\nu_\mu \to \nu_e) \approx 4 U^2_{\mu 3} U^2_{e3} \sin^2(\Delta m^2_{32}(1.27 L/E)) \qquad (13)$$

$$P_{\text{short}}(\nu_\mu \to \nu_\tau) \approx 4 U^2_{\mu 3} U^2_{\tau 3} \sin^2(\Delta m^2_{32}(1.27 L/E)) \qquad (14)$$

for the short oscillations, and

$$P_{\text{long}}(\nu_\mu \to \nu_e) \approx 4 U^2_{\mu 1} U^2_{e1} \sin^2(\Delta m^2_{21}(1.27 L/E)) \qquad (15)$$

$$P_{\text{long}}(\nu_\mu \to \nu_\tau) \approx 4 U^2_{\mu 1} U^2_{\tau 1} \sin^2(\Delta m^2_{21}(1.27 L/E)) \qquad (16)$$

for the long oscillations. If the mass hierarchy is valid, and, if the mixing matrix also obeys a generation hierarchy like the CKM matrix (*e.g.* $U^2_{e3} <$

[1] One can also consider an "inverted hierarchy" with $m_1 \ll m_2 \approx m_3$ where the relation $\Delta m^2_{21} \approx \Delta m^2_{31} > \Delta m^2_{32}$ is true.

$U^2_{\mu 3} < U^2_{\tau 3}$), then the probability $P(\nu_\mu \to \nu_e) \propto U^2_{e3}$ is expected to be smaller than the probability $P(\nu_\mu \to \nu_\tau) \propto U^2_{\tau 3}$ in the "short" oscillations and the opposite for the "long" oscillations.

However, it is possible that experimental results interpreted within the two-generation mixing formalism may indicate different Δm^2 scales with different apparent strengths for the same oscillation. This is because multiple terms involving different mixing strengths and Δm^2 values contribute to the transition probability for $\nu_\alpha \to \nu_\beta$.

2. Experimental situation

2.1. Neutrino oscillation experiments

There are two types of oscillation searches: "disappearance" and "appearance." We consider a pure source of neutrinos of type α. In a disappearance experiment, one looks for a deficit in the expected flux of ν_α. Appearance experiments search for $\nu_\alpha \to \nu_\beta$ by directly observing interactions of neutrinos of type β.

The case for oscillations is most convincing if the deficit or excess has the (L/E) dependence predicted by the neutrino oscillation formula. Experimentally, this has not yet been observed with strong statistical accuracy. Deficits have been observed in the expected rate of two neutrino sources: solar and atmospheric. A signal has been been observed by the LSND experiment, but it is not with high statistical significance and the L and E dependence has not yet been clearly demonstrated.

2.2. Experimental hints and evidence for neutrino oscillations

Three different sources of neutrinos have shown deviations from the expectation, consistent with oscillations. Figure 2 summarizes the allowed regions from these results.

- The first, called the **Atmospheric Neutrino Deficit**, refers to neutrinos produced by decays of mesons from cosmic ray interactions in the atmosphere. An observed anomalous ratio of ν_μ/ν_e can be interpreted as oscillations with $\Delta m^2 \sim 10^{-3}\mathrm{eV}^2$. A consistent picture has been seen in several ways by several experiments. The detailed fits to the angular distributions are a "smoking gun". The oscillation parameters are beginning to be pinned down. This effect is further discussed in Section 7.

- The second, called the **Solar Neutrino Deficit**, is a low rate of observed ν_e's from the Sun. The data are consistent with $\Delta m^2 \sim 10^{-10}\text{eV}^2$ or $\Delta m^2 \sim 10^{-5}\text{eV}^2$, depending on the theoretical interpretation. A large flux suppression has been seen by all experiments but the oscillation mass-angle region is not pinned down. There are still some questions about the solar model, but a purely astrophysical solution to the problem is highly disfavored. No "smoking guns" has been observed yet. This effect is further discussed in Section 6.

- The third observation is **an apparent excess of $\overline{\nu}_e$ events** in a $\overline{\nu}_\mu$ beam by the LSND experiment, with $\Delta m^2 \sim 1\text{eV}^2$. This result has been persistent for 5 years, but it is based on a single experiment. The mass-angle parameters are confined to a small remnant space not excluded by other experiments. This effect is awaiting a convincing confirmation or disproof. It is is further discussed in Section 4.

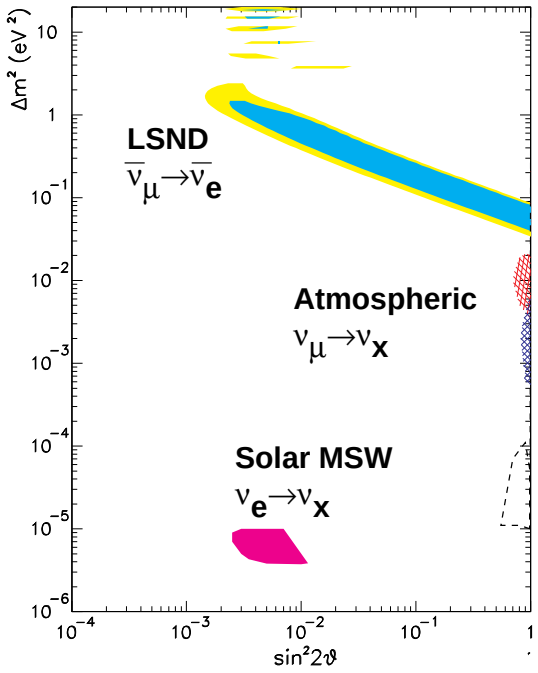

Fig. 2. Hints for oscillations come from solar neutrinos, atmospheric neutrinos and accelerator neutrinos (LSND). Allowed regions for these three indications are presented here interpreted with 2 neutrino mixing. The solar neutrino deficit has two possible oscillation solutions, MSW and vacuum (not shown in figure) with $\Delta m^2 \approx 10^{-10}$ eV^2.

The overall picture appears problematic. Indeed, we observe that we need three different Δm^2 regions in order to explain all experimental hints. With the three ordinary neutrinos, only two mass differences are independent one from another. In order to satisfy all experimental constraints, one must therefore invent new schemes with more neutrinos, like for example in the case of new sterile neutrinos. On the other hand, one can argue that one or more experimental results are incorrect.

The NOMAD [2] and CHORUS [3] experiments explore the high Δm^2 $\nu_\mu \leftrightarrow \nu_\tau$ oscillation region, where one may expect a signature from neutrinos which contribute to "dark matter" in the universe. Recent astrophysical data has indicated that some of the dark matter may be "hot." Massive neutrinos may be a good candidate for the hot component of the dark matter in the universe since the density of relic neutrinos from the Big Bang is $\sim$100 ν's/cm^3/type. Neutrinos in the mass range of $1 \sim 6$ eV could help to explain the small scale structure in the universe and recent anisotropy measurements of the photon background radiation. If one assumes that the heaviest neutrino is much more massive than the rest, then the astrophysical data indicate that the region of interest for searches is approximately $1 < \Delta m^2 < 36$ eV^2.

It should be noted that if neutrino masses do not follow a simple hierarchy, the sum of their masses can lie in eV range but the Δm^2's do not necessarily have to be large. The three ν_e, ν_μ and ν_τ components or two of the three could then significantly contribute to the hot dark matter mass.

Theses searches are further discussed in Section 3.

3. $\nu_\mu \to \nu_\tau$ searches at small mixing and high Δm^2

Before NOMAD and CHORUS experiments, the best limit in the high Δm^2 region was obtained in an emulsion experiment E531 [4] at Fermilab which found no evidence of the tau neutrino. Their limit for $\Delta m^2 \to \infty$ is $\sin^2 2\theta < 4 \times 10^{-3}$ at the 90% C.L.

It is experimentally challenging to find a small mixed fraction of ν_τ charged current interaction in a large amount of "standard" neutrino interactions. The two experiments use different techniques to identify the same events $\nu_\tau + N \to \tau + X$:

- **Vertex topology criteria**: CHORUS looks close to the primary vertex and given the micrometer resolution of the emulsion can directly detect the presence of the tau through the observation of a kink.

- **Kinematical criteria**: NOMAD does not have a good enough vertex resolution but relies on precise kinematical reconstruction of the tau decay products and the hadronic jet to separate backgrounds from signal events.

NOMAD and CHORUS took data at the CERN WANF beam. The beam component of this latter is shown in Table II. A comparison of their results is shown in Table III. The current situation with the latest NOMAD and CHORUS results is shown in figure 3, where all previous $\nu_\mu \to \nu_\tau$ oscillation searches are also summarized. All those searches are negative. The NOMAD and CHORUS experiments are further discussed in the following sections.

TABLE II

CERN WANF neutrino beam parameters at the NOMAD detector location (averaged over NOMAD fiducial volume).

	Flux		CC interactions	
Neutrino	$\langle E_\nu \rangle$[GeV]	relative ab.	$\langle E_\nu \rangle$[GeV]	relative ab.
ν_μ	23.5	1.0	41.5	1.0
$\bar{\nu}_\mu$	22.7	0.054	51.5	0.027
ν_e	36.9	0.0086	55.6	0.0134
$\bar{\nu}_e$	31.3	0.0026	52.1	0.0018

TABLE III

A comparison of the results from CHORUS and NOMAD. N_μ is the number of equivalent located events in the CHORUS emulsion used to compute their limit.

	CHORUS	NOMAD
Data sample:		
N_μ and ν_μ CC events	36182	950000
Sensitivity:		
$\langle \sigma_\tau / \sigma_\mu \rangle$	0.53	0.48
$\epsilon \times$ Br	0.14	0.018
$N_\mu \times \epsilon \times \text{Br} \times \langle \sigma_\tau / \sigma_\mu \rangle$	2644	8140
Total background	$\simeq 0.5$	23.8 ± 2.6
Candidates observed	0	21
Limit:		
$\sin^2 2\theta$ limit high Δm^2	1.8×10^{-3}	1.2×10^{-3}

3.1. NOMAD experiment

The NOMAD experiment (see figure 4) uses the UA1 magnet which provides a horizontal magnetic field of 0.4 T perpendicular to the beam axis over a volume of $3.6 \times 3.5 \times 7.0$ m^3. The main detector components are: *(i)* drift chambers which are used to reconstruct charged particle tracks and act as the neutrino target (mass of ~ 2.7 tons over a fiducial area of 2.6×2.6 m^2; average density 0.1g/cm^3); *(ii)* nine modules of transition radiation detec-

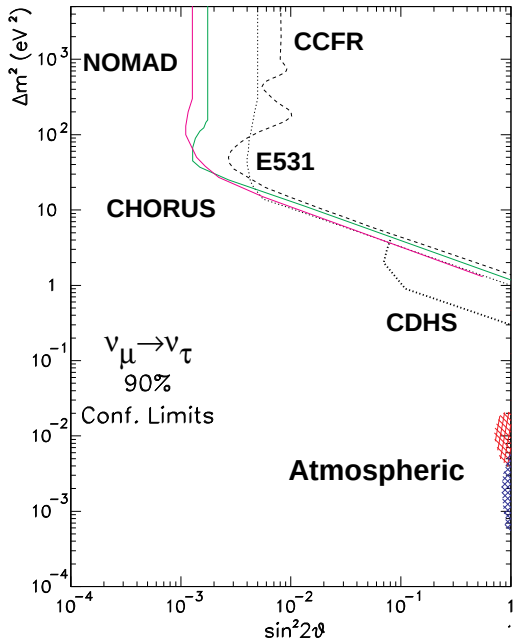

Fig. 3. Status of $\nu_\mu \rightarrow \nu_\tau$ oscillation searches in terms of two neutrino mixings. All the curves in the high Δm^2 region are limits while the region indicated as "Atmospheric" corresponds to the $\nu_\mu \rightarrow \nu_\tau$ oscillation interpretation of the Kamiokande and SuperKamiokande atmospheric neutrino results.

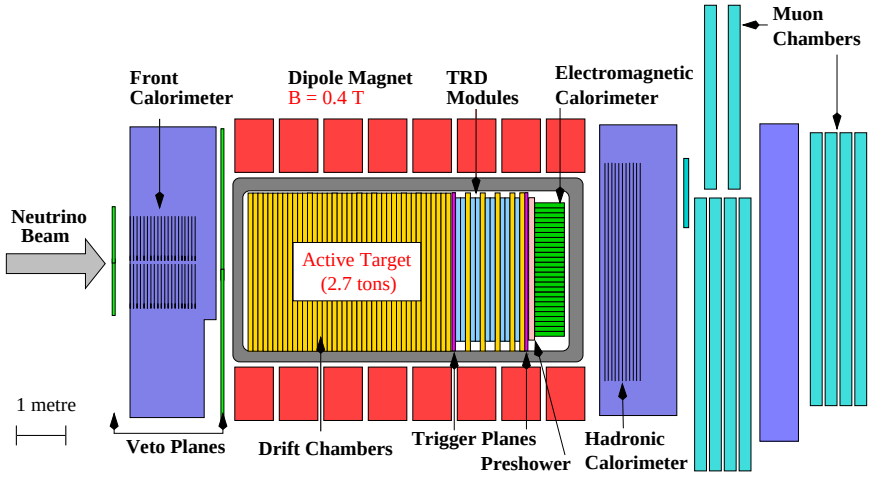

Fig. 4. Side view NOMAD detector.

tors (TRD) for electron identification; *(iii)* an electromagnetic calorimeter consisting of 875 lead-glass counters; *(iv)* a hadronic calorimeter made of a multi-layer iron-scintillator sandwich; *(v)* ten large-area muon chambers arranged in two stations separated by an 80 cm thick iron wall.

In order to exploit the low ν_e contamination of the wide band beam for the $\nu_\mu \to \nu_\tau$ search, the apparatus has been optimized to efficiently detect electrons and in particular ν_e charged current interactions (ν_eCC). Electron identification is performed using the transition radiation detector, preshower and the lead glass electromagnetic calorimeter. The preshower and the electromagnetic calorimeter provide additional π/e separation factor and an energy resolution $\sigma(E)/E = 3.2\%/\sqrt{E(\mathrm{GeV})} \oplus 1\%$ for electrons.

During the 1995-1997 years, a data sample corresponding to 950 000 ν_μ CC interactions has been accumulated. In addition, one expects 25000 $\bar{\nu}_\mu$ CC, 13000 ν_e CC, and 1700 $\bar{\nu}_e$ CC interactions, and approximately 310000 neutral current (NC) interactions. In addition, approximately 180000 ν_μ CC have been accumulated during the 1998 run and are currently being analyzed.

NOMAD relies on a careful study of the kinematics of these events. Particle isolation and momentum balance (especially in the transverse plane) at the primary vertex allow to distinguish the ν_τ CC interactions from ν_μ and ν_e CC or NC background events. The following τ^- decay channels are considered: the electronic channel $e^-\nu_\tau\bar{\nu}_e$, and the hadronic ones: $\pi^-\nu_\tau$, $\rho^-\nu_\tau$ and $\pi^-\pi^-\pi^+ n\pi^0\nu_\tau$, *i.e.* about 80% of the τ decays.

The kinematical technique used by NOMAD is illustrated with two examples. First we consider the identification of τ candidates which decay as $\tau^- \to \nu_\tau e^- \overline{\nu}_e$. This mode is particularly attractive because the main background results from ν_e CC events which are $\sim 1\%$ of the total number of neutrino interactions. The difference between the two types of events is illustrated in figure 5. For each event, the sum of the momenta transverse to the beam direction for visible particles is calculated and the resulting missing transverse momentum vector $\vec{p}_{\mathrm{T}}^{\,\mathrm{miss}}$ is reconstructed. The relevant quantities are then P_{T}^{τ}, the transverse momentum of the observed electron, P_{T}^{H}, the transverse momentum of the hadronic jet and $\vec{p}_{\mathrm{T}}^{\,\mathrm{miss}}$, the missing transverse momentum. In the case of a ν_τ CC this missing transverse momentum is essentially due to the undetected neutrinos emitted in the τ decay, while in the case of a ν_e CC it is due to undetected neutrals, reconstruction effects, and the Fermi motion.

No single kinematical variable unambiguously signals the presence of a τ lepton. Instead one exploits the fact that the distributions of several kinematical variables are different for the τ signal and the various backgrounds. Therefore, information is optimized by combining these variables into a likelihood ratio function.

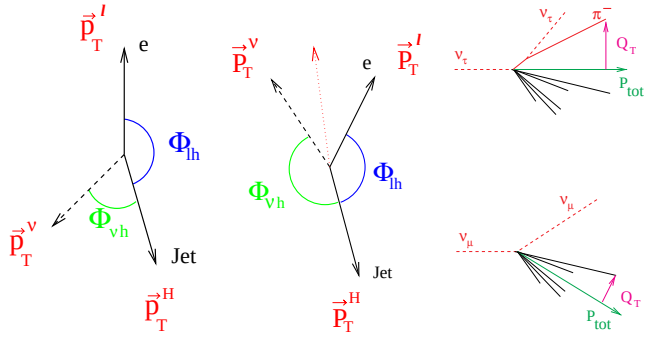

(a) ν_e CC (b) ν_τ CC (c) $Q_{\rm T}$ variable

Fig. 5. Kinematical triangle in the transverse plane of the event (a) for background (b) for signal. (c) Isolation of the τ daughter candidate for ν_μ NC and ν_τ CC events.

To classify electron events, two likelihood functions were used. The first is designed to distinguish $\tau^- \to e^- \bar{\nu}_e \nu_\tau$ signal events from ν NC background. It is formed from 2D and 3D distributions (thereby including correlations) of combinations of many variables, *i.e.* the angle between the neutrino direction and the reconstructed total energy vector $\theta_{\nu p}$, the angle between the neutrino direction and the hadronic jet $\theta_{\nu H}$, the angular isolation of the candidate $\theta_{\rm iso}$, the electron kinematical isolation $Q_{\rm T} = \sqrt{(P^\tau_{\rm T})^2 - (P^\tau_{\rm T} \cdot \vec{P^{}_{\rm tot}})^2 / P^2_{\rm tot}}$, the total visible energy $E^{\rm tot}_{\rm e}$, and the transverse mass $M_{\rm T}$. For each event, the likelihood ratio $\ln \lambda_{e1}$ of signal events and of ν NC events is computed. High values of this ratio effectively select electrons isolated from the hadronic jets.

The second function is designed to distinguish $\tau^- \to e^- \bar{\nu}_e \nu_\tau$ signal events from ν_e CC background. It is formed from the product of two 3D distributions: ($P^\tau_{\rm T}$, $P^H_{\rm T}$, ϕ_{eH}) and ($E_{\rm vis}$, $\theta_{\nu p}$, the transverse momentum of the electron w.r.t. to the hadron jet $Q_{\rm Lep}$). For each event, a likelihood ratio $\ln \lambda_{e2}$ constructed from signal events and from ν_e CC events is defined.

The combined rejection power of the two likelihood ratios can be seen in figure 6, which is a scatter plot of $\ln \lambda_{e2}$ vs $\ln \lambda_{e1}$, for MC simulations of signal and backgrounds. The large boxed region at large values of both ratios contains little background but is populated by signal events. It is subdivided into five "sub-boxes" which have varying signal-to-background ratios. Figure 7 shows the distribution of $\ln \lambda_{e2}$, for events passing all cuts except the one on $\ln \lambda_{e2}$, for the sum of simulated backgrounds, the $\tau^- \to e^- \bar{\nu}_e \nu_\tau$ simulation (arbitrarily normalized), and the 1995-1997 data, in good agreement with background expectations.

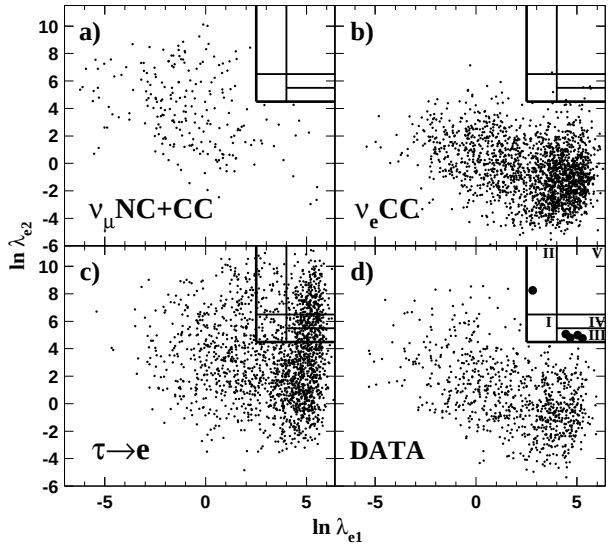

Fig. 6. Scatter plot of $\ln\lambda_{e2}$ vs $\ln\lambda_{e1}$ for (a) MC ν_μ NC (and the few surviving ν_μ CC), (b) MC ν_e CC, (c) MC $\tau^- \to e^-\bar{\nu}_e\nu_\tau$, and (d) data (the large full circles represent the five surviving events in the box). The large box at the upper right corner indicates the signal region and is divided into sub-boxes.

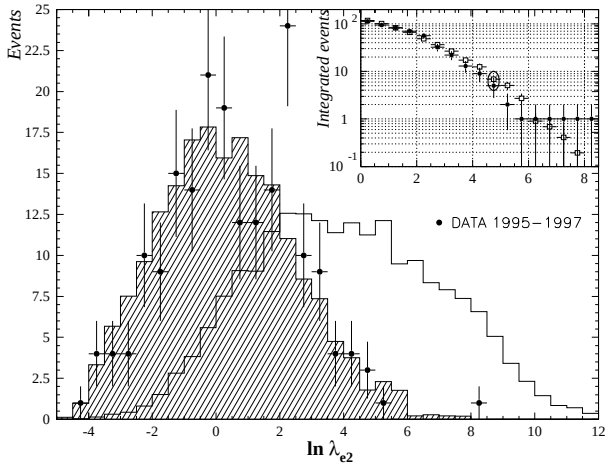

Fig. 7. Histogram of $\ln\lambda_{e2}$ for events passing all cuts except the one on $\ln\lambda_{e2}$, for sum of simulated backgrounds (shaded), $\tau^- \to e^-\bar{\nu}_e\nu_\tau$ simulation (unshaded), and data (points with statistical error bars). The inset gives, for each value of $\ln\lambda_{e2}$, the total number of events beyond that value, for data (dots) and expected background (squares); the encircled points are at the boundary of the signal region.

The analysis of the τ hadronic decays relies mainly on isolation and angular cuts and proceeds in three steps: the selection of the hadron candidate; the rejection of ν_μ, $\bar{\nu}_\mu$, ν_e, and $\bar{\nu}_e$ CC interactions; and the final separation of the signal from the background by means of kinematic criteria. Particle identification is used to reject events containing primary electrons or muons. The main backgrounds are ν induced neutral currents. For example, for the single pion decay, one pion from the hadronic jet is mistaken as the pion emanating from the τ decay. The most relevant kinematical difference between the τ signal and the NC background is the isolation of the τ daughter candidate w.r.t. the hadronic jet (see figure 5), which can be described with the variable

$$Q_{\rm T} = \sqrt{(P_{\rm T}^{\tau})^2 - (P_{\rm T}^{\tau} \cdot \vec{P_{\rm tot}})^2 / P_{\rm tot}^2}\,. \tag{17}$$

We illustrate the search for $\tau^- \to h^-(n\pi^0)\nu_\tau$ decays, where h^- is a hadron and $n \geq 0$. The kinematic criteria used to reject the residual backgrounds are based on five variables $Q_{\rm T}, M_{\rm T}, p_{\rm T}^H, \rho_m, y_{\rm Bj}$ where:

$$\rho_m = \frac{p_{\rm T}^m}{(p_{\rm T}^m + p_{\rm T}^\tau + p_{\rm T}^H)}, y_{\rm Bj} = \frac{p^H}{(p^\tau + p^H)}\,.$$

The distribution of the logarithm of the ratio between signal and background likelihoods, $\ln \lambda_{h\rm kin}$, is shown in figure 8(b) for backgrounds and signal separately. Distributions of $Q_{\rm T}$ and ρ_m are shown in Figs. 8(c) and 8(d), respectively (these two variables provide the highest rejection power against NC background).

Figure 8(e) shows the number of h^- events above a given $\ln \lambda_{h\rm kin}$ value for the predicted background normalized to the total number of ν_μ CC interactions in the data, and the number of events in the data. The signal box is defined as $\ln \lambda_{h\rm kin} > 7$.

The corresponding distributions for h^+ events are shown in figure 8(f). It can be seen from Figs. 8(e) and 8(f) that the data agree with the predicted background outside the signal box for h^-, and everywhere for h^+.

The NOMAD analyses have so far used the 1995-1997 data. Studies of the 1998 sample are under progress. The result from all channels are summarized in Table IV. The candidate events found are consistent with the total estimated backgrounds.

The resulting 90% C.L. upper limit on the oscillation probability is

$$P_{\rm osc}(\nu_\mu \to \nu_\tau) < 0.6 \times 10^{-3}, \tag{18}$$

which corresponds to $\sin^2 2\theta_{\mu\tau} < 1.2 \times 10^{-3}$ for large Δm^2.

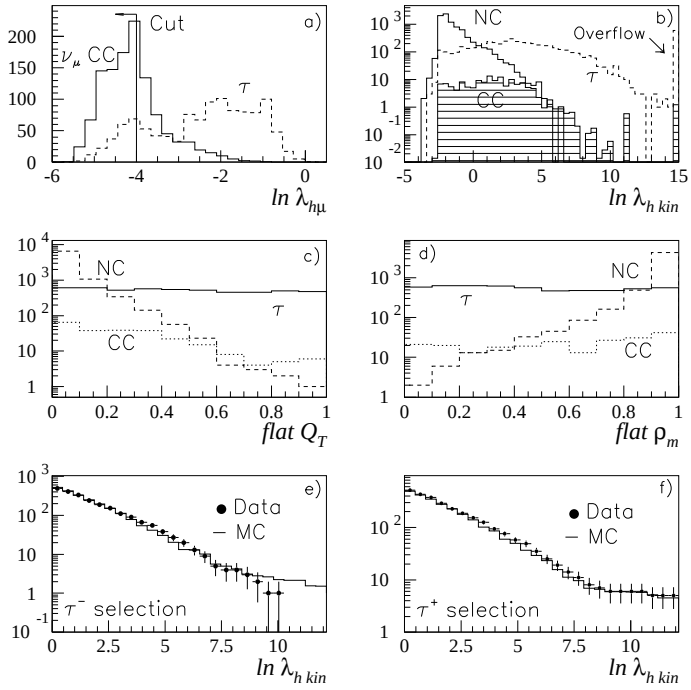

Fig. 8. Distributions from the search for $\tau^- \to h^-(n\pi^0)\nu_\tau$: (a) $\ln\lambda_{h\mu}$ for ν_μ CC background and for signal; (b) $\ln\lambda_{h\,\mathrm{kin}}$; (c) Q_T, after transformation to the metric in which the signal density is uniform from 0 to 1; (d) ρ_m, after transformation to the metric in which the signal density is uniform from 0 to 1; (e) the integrated number of h^- events above a given $\ln\lambda_{h\,\mathrm{kin}}$ value for the predicted background and for the data; and (f) the corresponding plot for the τ^+ control search. The uncertainty on the background predictions in (e) and (f) is similar to that of the data points.

3.2. CHORUS experiment

In order to analyze their events, CHORUS must traceback interesting events from the predictions given by the electronic detectors into the bulk emulsion to locate the neutrino vertex (see figure 9). After development of the emulsions, the events are measured in the scanning laboratories using fully automatic microscopes. Two separate analyses have been performed so far: the search for $\tau \to \mu\nu\nu$ ($1-\mu$ sample) and the search for $\tau \to h^-(n\pi^0)\nu$ ($0-\mu$ sample).

For the first search, all events with an identified negative muon with momentum $P_\mu < 30$ GeV are selected. Scanned statistics are shown in Table V.

TABLE IV

Summary of backgrounds and efficiencies for the NOMAD tau analyses. The column τ^- summarizes the observed number of τ^- candidate events and the corresponding predicted background for each channel. The column τ^+ contains the equivalent numbers for "wrong sign" candidates. The corresponding τ^- selection efficiencies (ϵ) and τ branching ratios (Br) are also listed. The maximum number of expected signal events ($N_\tau^{\max}$) is indicated for each channel. LM refers to low-multiplicity analyses (see Ref. [2]).

	τ^-		τ^+				
Analysis	Data	MC	Data	MC	$\epsilon(\%)$	Br(%)	$N_\tau^{\max}$
$\tau \to e$	5	$6.3^{+1.6}_{-1.0}$	7	7.4 ± 3.1	3.5	17.8	2818
$\tau \to h(n\pi^0)$	5	5.0 ± 1.2	14	9.9 ± 2.3	0.78	49.8	1727
$\tau \to \rho$	5	$5.0^{+1.7}_{-0.9}$	13	$10.2^{+1.4}_{-1.1}$	1.6	25.3	1891
$\tau \to 3\pi(\pi^0)$	5	6.5 ± 1.1	14	13.5 ± 1.4	2.9	15.2	1180
$\tau \to e$ LM	0	$0.5^{+0.6}_{-0.2}$	1	1.1 ± 0.7	3.4	17.8	218
$\tau \to \pi(\pi^0)$ LM	1	$0.1^{+0.3}_{-0.1}$	6	8.8 ± 3.5	1.5	37.3	198
$\tau \to 3\pi(\pi^0)$ LM	0	$0.4^{+0.6}_{-0.4}$	14	11 ± 4	2.0	15.2	108

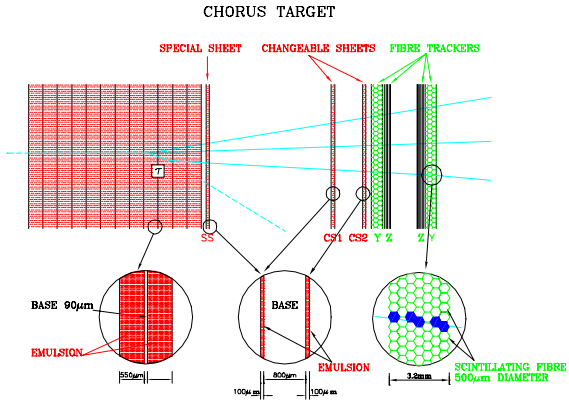

Fig. 9. Schematic view of the CHORUS experiment target. The event is located in the bulk emulsion via a prediction made by electronic detector and with the help of changeable emulsion sheets.

The muon track is automatically followed in the emulsion until the neutrino interaction vertex is reached. The *decay search* is done in two different ways:

- the short decay search (see figure 10): inside the plate where the interaction took place, the impact parameter of the muon is evaluated at the minimum distance between the track and any other track of the event.

TABLE V

Results from 1μ-sample search in CHORUS.

	1994	1995
Data:		
Charged current expected	120000	200000
1μ sample	95374	155558
$P_\mu < 30$ GeV	66911	110916
Scanned so far	41931	37569
Fiducial cuts	35767	32046
Vertex found in emulsion	16837	14586
Total	31423	
Backgrounds:		
Charm	0.05	

TABLE VI

Results from 0μ-sample search in CHORUS.

	1994	1995
Data:		
0μ sample	50383	71595
Scanned so far	8908	12365
Fiducial cuts	5476	6920
Vertex found in emulsion	3164	3680
Total	6844	
Backgrounds:		
White-kinks ($P_{\rm T} > 250$ MeV)	$\simeq 0.5$	
Charm in $\bar{\nu}_\ell$ CC	0.02	
Wrong sign hadrons	0.03	

- the long decay search: the direction of the muon measured in the plate downstream is compared to the one measured by the scintillating fiber tracker. If the $P_t \approx \Delta\theta \times P_\mu$ is larger than 250 MeV, the event is manually scanned. Those events with a decay signature (kink) or a decay with $P_t > 250$ MeV are considered as tau candidates.

The backgrounds are small; they are induced by charm production by anti-neutrinos in the beam $\bar{\nu} + N \to {}^- + D^- + X$ followed by $D^- \to \mu^- + X'$ where the primary lepton escapes detection or is misidentified as a hadron. In the current sample, this background is estimated to be 0.05 events.

The 1-prong decay channel has a large branching of 50% but suffers from white-kinks background. A sample of 6844 muon-less events has been analyzed (see Table VI) using a kink-finding procedure similar to that of the muon channel. The hadron candidate is a negative hadron track with momentum $1 < P < 20$ GeV. With the current statistics, the charm back-

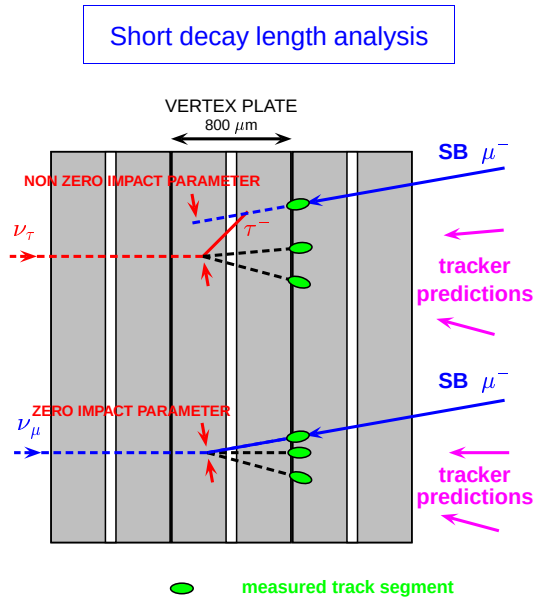

Fig. 10. Schematic representation of the search for kinks in CHORUS.

ground is negligible — 0.02 events. The important background results from recoilless elastic scattering of hadrons against the heavy nuclei in the emulsion (white-kinks). The cross-section for this process is divergent for the scattering angle going to zero. It fortunately has an exponential p_t fall-off and can therefore be suppressed by an appropriate p_t cut at a small cost of tau efficiency. The amount of background can be estimated by looking in the data at "far" white-kinks along the hadron track, since genuine tau decays should occur with a mean decay length of about 1 mm. In the analyzed sample, this background is estimated to be about 0.5 event. After the p_t cut, no event survives in the sample (3 events had observable kinks). Further kinematical criteria at the vertex are expected to help suppress this background at a modest tau efficiency cost.

After human assisted scanning, no tau candidates have been found in the samples. The limit on the probability of $\nu_\mu \to \nu_\tau$ oscillations is calculated to be:

$$P(\nu_\mu \to \nu_\tau) < 0.9 \times 10^{-3} \tag{19}$$

which corresponds to $\sin^2 2\theta_{\mu\tau} < 1.8 \times 10^{-3}$ for large Δm^2 at the 90% C.L. The kink efficiency, potential source of the largest systematic error, has been estimated from Monte-Carlo studies. With larger statistics, a cross-check of the kink efficiency will be performed using charm events.

4. The LSND signal

4.1. The LSND and KARMEN apparatus

The LSND experiment consists of a steel tank filled with 167 tons of liquid scintillator located at about 30 m from the source. The tank is viewed by 1220 uniformly spaced 8″ PMT's covering 25% of the surface. The scintillator medium consists of mineral oil (CH_2) with a small admixture (0.031 g/l) of butyl-PBD. This mixture allows the detection of both Čerenkov and isotropic scintillation light.

In KARMEN, the oscillation channels $\nu_\mu \to \nu_e$ and $\bar{\nu}_\mu \to \bar{\nu}_e$ are investigated with 56 tons of liquid scintillator contained in a matrix of 512 independent counters located at a mean distance of 17 m from the source. A thin layer of Gd_2O_3 placed between adjacent counters allows neutron detection by neutron capture in Gadolinium followed by γ emission with a total energy of ~ 8 MeV.

The main features of the two experiments are compared in Table VII.

TABLE VII

The comparison between LSND and KARMEN experimental setups.

	LSND	KARMEN
Beam:		
Accelerator	LAMPF	ISIS
Energy	800 MeV	800 MeV
Proton current	1mA	0.2 mA
Beam pulse	$500\mu s$	2×100 ns
	8.3ms pause	20ms pause
Detector:		
Mass	180t	56t
Detection	liquid scintillator	segmented
	+ Čerenkov	liquid scintillator
Neutron capture	proton	Gd
	2.2 MeV γ	8 MeV γ
Oscillations:		
E (MeV)	20-300	20-60
L (m)	29	17
Angle from beam axis	17^o	90^o

In 1996, the KARMEN experiment has been upgraded by an additional veto system. Vetoing of cosmic muons passing the 7000 ton massive iron shielding of the detector suppresses energetic neutrons from deep inelastic scattering of muons as well as from μ-capture in iron. Until the upgrade, these neutrons penetrating into the detector represented the main background for the $\bar{\nu}_\mu \to \bar{\nu}_e$ oscillation search. With an expected reduction of

the background rate by a factor 40, the experimental sensitivity for $\bar{\nu}_\mu \to \bar{\nu}_e$ has been enhanced.

The LSND hint for neutrino oscillations is the only indication for oscillations which is a *signal*, as opposed to a deficit. Evidence has been seen for both $\bar{\nu}_\mu \to \bar{\nu}_e$ and $\nu_\mu \to \nu_e$ oscillations. In 1995 the LSND experiment published data showing candidate events that were consistent with $\bar{\nu}_\mu \to \bar{\nu}_e$ oscillations [5]. Additional event excesses were published in 1996 and 1998 for both $\bar{\nu}_\mu \to \bar{\nu}_e$ oscillations and $\nu_\mu \to \nu_e$ oscillations [6]. The two oscillation searches are complementary, having different backgrounds and systematics, yet yielding consistent results. A comparison of the energy dependence of the observed $\overline{\nu}_e$ events and the non-beam background indicates a "Fitted Excess" of events as shown in Table VIII. Comparing this "Fitted Excess" to the expected $\overline{\nu}_e$ beam background then yields a "Total Excess" for the decay-at-rest analysis, summarized in Table VIII, and shown by the allowed regions in figure 11.

TABLE VIII

Preliminary numbers of excess events and the corresponding oscillation probabilities for the running periods 1993–1995, 1996–1997, and 1993–1997.

Data Sample	Fitted Excess	$\bar{\nu}_e$ Backgnd	Total Excess	Osc. Prob.
1993-1995	63.5 ± 20.0	12.5 ± 2.9	51.0 ± 20.2	$(0.31 \pm 0.12 \pm 0.05)\%$
1996-1997	35.1 ± 14.7	4.8 ± 1.1	30.3 ± 14.8	$(0.32 \pm 0.15 \pm 0.05)\%$
1993-1997	100.1 ± 23.4	17.3 ± 4.0	82.8 ± 23.7	$(0.31 \pm 0.09 \pm 0.05)\%$

In the data collected through 1997 and 1998 no potential oscillation event was observed in KARMEN2 [7]. Using the Unified statistical approach [8], this leads to an upper limit for the mixing angle of $\sin^2(2\theta) < 1.3 \times 10^{-3}$ (90% C.L.) at large Δm^2 covering almost entirely the favored region defined by the LSND evidence. KARMEN2 after all cuts observed 0 events while 2.88 ± 0.13 background events are expected (this has a 5.6% probability of occurring as a statistical fluctuation)! A typical signal for the $\Delta m^2 < 1$ eV^2 region is 1 event, if LSND is correct. There is disagreement on how to handle data in the case of background plus a small expected signal. When the background fluctuates low there can be significant differences in results depending on the statistical approach used. The unified approach used by KARMEN2 sets the limit as $\mu_{90\%C.L.} = 1.1$ events. The experimental sensitivity is 4.4 events which is worse than the limit by a factor of four.

A more conservative alternative is to use a Bayesian approach. If less background is observed than expected, one may be overestimating the background. Therefore one should set a limit assuming that the background is zero. Therefore this method sets the limit at 2.3 events, a limit about twice worse than the Unified Approach result.

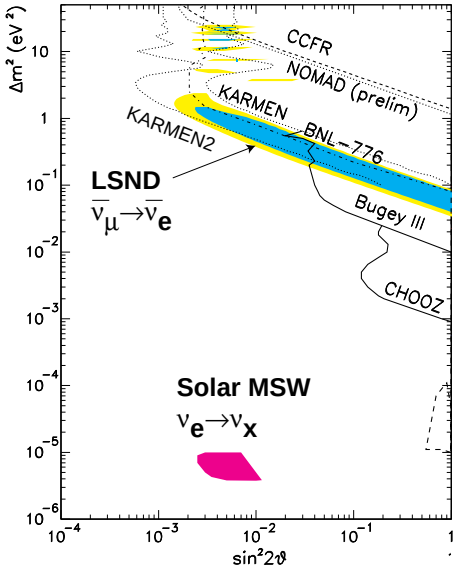

Fig. 11. Status of $\nu_\mu \to \nu_e$ oscillation searches in terms of new neutrino mixing. All the curves are limits while the shaded region indicates the regions corresponding to the oscillation interpretation of the LSND result. The latest result from KARMEN is indicated as KARMEN2.

The goal now should be high statistics, low systematics experiments designed to address the hints for oscillations which have been observed.

5. Future tests of the LSND signal

In order to confirm the result from LSND, it is mandatory to observe the *energy-dependent modulations* in the disappearance and appearance rates. The issues related to the LSND signal are: Is the signal due to oscillations? What is the Δm^2? What is the $\sin^2 2\theta$? What is required at this point is an experiment which definitively covers the entire LSND allowed region with large statistical significance and which could measure the oscillation parameters.

5.1. BooNE and MiniBooNE at Fermilab

BooNE [9] (Booster Neutrino Experiment), which has been approved at FNAL, will be capable of observing both $\nu_\mu \to \nu_e$ appearance and ν_μ disappearance. The first phase, MiniBooNE, is a single detector experiment designed to obtain $\sim$ 1000 events per year if the LSND signal is due to $\nu_\mu \to \nu_e$ oscillations. This establishes the oscillation signal at the $\sim 8\sigma$

level. The second phase of the experiment introduces a second detector, with the goal to accurately measure the Δm^2 and $\sin^2 2\theta$ parameters of observed oscillations.

MiniBooNE will begin taking data in 2001. The detector will consist of a spherical tank 6 m in radius. An inner structure at 5.5 m radius will support 1220 8-inch phototubes (10% coverage) pointed inward and optically isolated from the outer region of the tank. The vessel will be filled with 769 ton of mineral oil, resulting in a 445 ton fiducial volume. The outer volume will serve as a veto shield for identifying particles both entering and leaving the detector, with 292 phototubes mounted on the support structure facing outwards. The first detector will be located 500 m from the Booster neutrino source. The neutrino beam, constructed using the 8 GeV proton Booster at FNAL, will have an average beam energy of approximately 0.75 GeV.

The sensitivity to oscillations can be calculated by summing over energy or by including energy dependence in the fit. As shown in figure 12, both the summed analysis and the energy-dependent analysis extend well

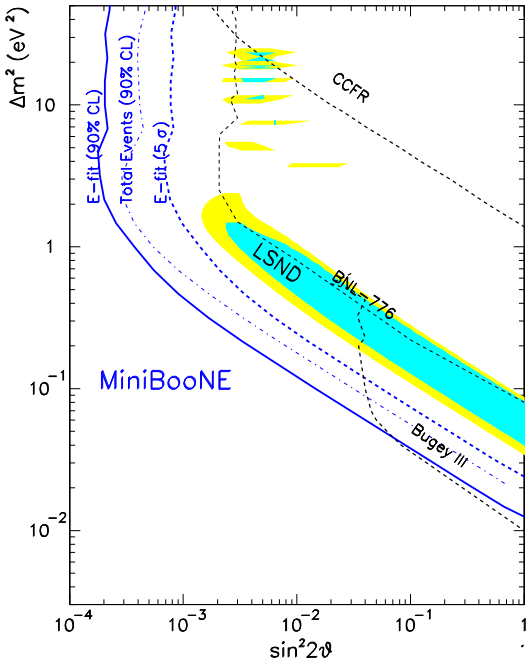

Fig. 12. Expected sensitivity regions for the MiniBooNE experiment with 5×10^{20} protons on target (1 year). The solid (dashed) curve is the 90% C.L. (5σ) region using the energy fit method and the dashed-dot curve is the 90% C.L. region using the total event method.

beyond the LSND allowed region at 90% C.L. Also shown is the region where MiniBooNE will see a 5σ or greater signal above background and make a conclusive measurement, which again extends well beyond the LSND signal region.

5.2. Proposals at CERN

The Jura mountain position at 17 km [10] from the continuation of the existing neutrino beamline at CERN has essentially the exact L/E to perform a test of the LSND claim. In addition, relative to any other existing or planned facility, it offers two fundamental advantages: 1) the energy of the beam can be lowered by perhaps as much as an order of magnitude still allowing reasonable counting rates, at least in the $\nu_\mu \to \nu_e$ channel. It would be then possible to extend the search at higher L/E. 2) at the lowest value of the L/E the neutrino beam is comfortably above threshold for τ production. This allows a simultaneous study of the $\nu_\mu \to \nu_e$ and $\nu_\mu \to \nu_\tau$ channels, albeit in a somewhat more restricted L/E range because of the threshold effect.

ICARUS at Jura: The ICARUS-CERN-Milano groups have submitted a proposal [11] based on an exposure at the Jura of a 600 ton ICARUS [12] module similar to the one built for the Gran Sasso, resulting in an extended search for neutrino oscillations in the $\nu_\mu \to \nu_e$ and $\nu_\mu \to \nu_\tau$ appearance channels. Given the possible improved performances of the CERN neutrino beams, a fiducial mass of 100 tons would in fact be sufficient to test the LSND solution.

CERN/I216 [13]: Another possibility has been proposed at CERN to lower the energy of the neutrino beam by reactivating the old CERN PS neutrino beam.

Muon storage rings: The possibility to use the neutrino beam from muon decay to test the LSND signal has been studied [14, 15]. This is discussed in more details in Section 10.

6. Solar neutrinos

Solar neutrino experiments have observed the flux of neutrinos produced in the core of the the Sun in its fusion reactions. The rate is computed using solar models, of which the Standard Solar Model of Bahcall-Pinsonneault [16] is the reference. The predicted neutrino flux as a function of energy is shown in figure 13.

6.1. Flux measurement

The first observation of solar neutrinos was performed on chlorine by Davis and collaborators [17] in the Homestake experiment The threshold for

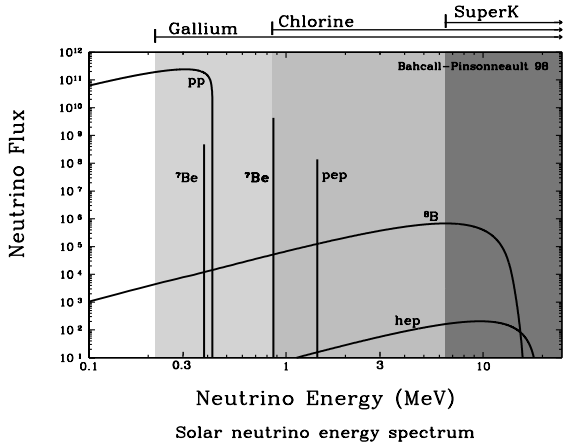

Fig. 13. Solar Neutrino Energy Spectrum (BP98 [16]). The origin of the neutrinos are indicated by the name of the reaction involved (*pp*, ^{7}Be, ^{8}B, *pep*, *hep*). The experimental thresholds are shown as well.

the reaction $\nu_e + {}^{37}\mathrm{Cl} \rightarrow {}^{38}\mathrm{Ar} + e^-$ is 860 KeV. Since then, Kamiokande, SuperKamiokande, GALLEX and SAGE experiments have measured the solar neutrino flux.

The Kamiokande [18] and SuperKamiokande experiments, using water as target, look for electron scattering $\nu_e + e \rightarrow \nu_e + e$ where the scattered electron is detected and measured. Experimental backgrounds considerations limit these studies to a threshold of about $5 - 6$ MeV. The signal from the Sun is extracted from a large irreducible background by an event-by-event angular correlation between the scattered electron direction and the direction of the Sun at the time of the event. This correlation can be done since events, unlike in the radio-chemical experiments, are accumulated real-time.

The SAGE and GALLEX experiments [19] use the $\nu_e + {}^{31}\mathrm{Ga} \rightarrow {}^{32}\mathrm{Ge} + e^-$ reaction with threshold as low as 233 KeV. This makes these experiments sensitive to the neutrinos coming from the main *pp* chain which is directly related to the luminosity of the Sun. Assuming that the rate of nuclear reaction does not exhibit a time dependence on the scale of a million year, one can directly relate the visible luminosity to the rate of *pp* reactions.

As shown in figure 14, all experiments measured a deficit in the solar neutrino flux. For both the experimental values and the predictions, the 1 sigma uncertainties are indicated by crosses. Many attempts have been performed to explain this deficit without invoking new physics. But after many years, the confidence in the SSM has grown very strong. In particular, helioseismology provides an excellent fit the to predicted values by the SSM (see Refs. [16, 20]). A purely astrophysical solution to the solar neutrino

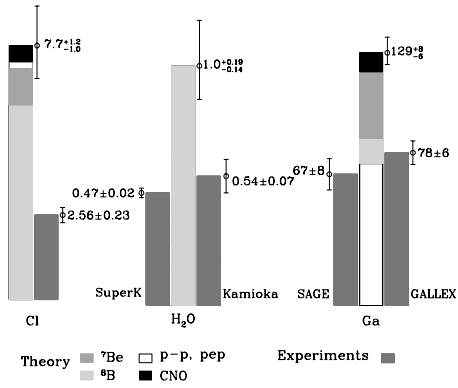

Fig. 14. Comparison of the predictions of the standard solar model with the total observed rates in the five solar neutrino experiments: chlorine, SuperKamiokande, Kamiokande, GALLEX, and SAGE (from BP98 [16]). For both the experimental values and the predictions, the 1 sigma uncertainties are indicated by crosses.

problem is highly disfavored [21].

6.2. Deficit interpreted as neutrino oscillation

It is tempting to invoke neutrino oscillations to solve the solar neutrino deficit. The deficit is interpreted as the disappearance of electron neutrino. Since experiments detect charged current reactions only, this will lead to apparent suppression of the flux. It is striking fact that the suppression factors are large, with average value of 0.5 for the water (Kamiokande: 0.54 ± 0.07 and SuperK: 0.47 ± 0.02) and gallium experiments. This suppression would appear naturally for maximally mixed neutrinos with an oscillation wavelength much smaller than the distance between the Earth and the Sun. In this case, no oscillation pattern is expected because the average of the fast oscillation yields a suppression factor of 1/2 over the full energy spectrum of the solar neutrinos.

However, the Homestake experiment seem to favor a suppression factor of about 0.33. This seems to indicate that the suppression factor depends on the solar neutrino energy. A global fit must be performed in order to include the different energy thresholds of the various experiments.

The energy dependence of the suppression forces the Δm^2 parameter to be constrained within a well defined region. If neutrino oscillations are occuring over the distance between the Sun and the Earth and variation of this oscillation seem to be visible by combining the solar neutrino experiments implies that the oscillation wavelength and the distance Sun-Earth must be comparable. In terms of mass difference, this gives $\Delta m^2_{\rm solar} \approx 10^{-10}{\rm eV}^2$.

MSW (Mikheyev–Smirnov–Wolfenstein) [22] effect occurs because the electron neutrino has both charged- and neutral-current elastic scattering with electrons, while the ν_μ and ν_τ experience only neutral-current scattering. When the neutrino propagate in matter (like for instance when travelling through the Sun), the additional interactions introduce a shift in the effective mass state. This leads to an increase in the oscillation probability:

$$P\left(\nu_e \to \nu_\mu\right) = \left(\sin^2 2\theta / W^2\right)\ \sin^2\left(1.27 W \Delta m^2 L/E\right)\ , \qquad (20)$$

where $W^2 = \sin^2 2\theta + (\sqrt{2} G_F N_e (2E/\Delta m^2) - \cos 2\theta)^2$ and N_e is the electron density. In a vacuum, where $N_e = 0$, this reduces to the standard equation. Within the sun, where the electron density varies from high values in the core decreasing towards the outer regions, "MSW resonances", or large enhancements of the oscillation probability can occur.

6.3. SuperKamiokande energy distribution measurement

A model-independent way of testing the oscillation hypotheses is to study the energy spectrum, the day–night and the seasonal variation of the solar flux, rather than relying on flux measurements alone. SuperKamiokande has measured the recoil electron spectrum above 5.5 MeV.

A convenient way to search for spectral distortions is to normalize the observed spectrum by the SSM expectations. A flavor oscillation hypothesis leads to deviations from a flat normalized spectrum. The strongest deviations are expected for "vacuum oscillations" at small Δm^2 . Matter-enhanced (MSW) neutrino oscillations show smaller deviations. In particular, the large-angle solution expects an almost flat normalized spectrum. The small-angle solution leads to a sloped normalized spectrum (low recoil energy bins are more strongly suppressed than high energy bins).

Figure 15 shows the latest measurement from SuperKamiokande based on 419 days of a new "Super-Low-Energy" analysis above an energy of 5.5 MeV and on the full 708 days for the rest of the events above 6.5 MeV. The expected suppressions for a vacuum solution ($\Delta m^2 = 4.3 \times 10^{-10}$ eV^2 and $\sin^2 2\theta = 0.87$ and two MSW solutions ($\Delta m^2 = 7.9 \times 10^{-6}$ eV^2 and $\Delta m^2 = 5 \times 10^{-6}$ eV^2 with mixing $\sin^2 2\theta = 6.3 \times 10^{-3}$) are overlayed on the experimental data.

The results obtained by SuperKamiokande on the electron spectrum came at first as a surprise. Indeed, the spectrum did show a deviation from expectation, in support for an oscillation scenario. Unfortunately, the oscillation parameters indicated by the fit of the electron spectrum did not agree well with the parameters found by the combined fit of the *suppression* of the fluxes obtained by the four experiments. The results of the combined fit are further discussed in Section 6.6.

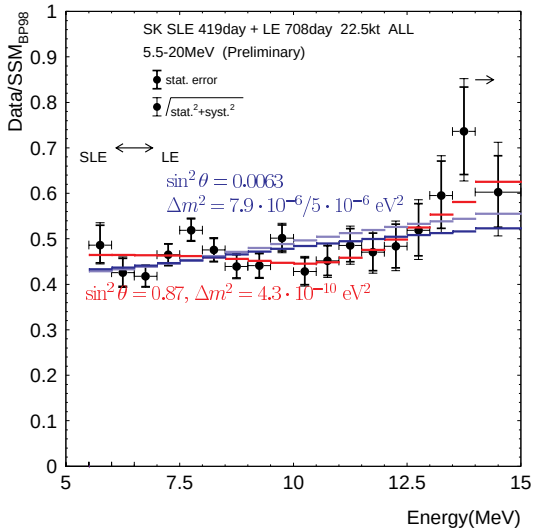

Fig. 15. Measured electron recoil spectrum from SuperK (708 days days) normalized to BP98 [16] expectations. The expected suppressions for a vacuum and two MSW solutions are overlayed on the experimental data.

A further complication came from the realization [23] that the prediction at high energy, *i.e.* in the region where the deviation from expectation appeared, the *hep* mechanism (see figure 13), if underestimated by a large factor of 20, could be a non negligible source of neutrinos that would explain the electron spectrum.

If one conservatively assumes that the only reliable region of the spectrum lies below 12 MeV, one can naively conclude from the figure that the spectrum does not exhibit an energy dependent suppression and that therefore deviations from the expected energy distribution has not been conclusively observed.

6.4. SuperKamiokande day-night asymmetry

MSW oscillations predict an enhancement of the solar neutrino flux during the night when the neutrinos pass through the earth. SuperKamiokande has looked for such an effect. The measured day–night asymmetry defined as

$$\frac{\text{day} - \text{night}}{\text{day} + \text{night}} = -0.026 \pm 0.016(\text{stat.}) \pm 0.013(\text{syst.})$$

does not significantly differ from zero. This result constrains so strongly the large mixing angle MSW solution that this solution disappears completely

at the 99% C.L. We are left with the small mixing angle MSW solution as the only viable solution that fits the overall observations.

6.5. SuperKamiokande seasonal variation

Since the distance Sun-Earth changes with a yearly cycle, vacuum oscillations can show a seasonal variation of the neutrino flux. This variation should be observed above the natural variations due to the eccentricity of the orbit of Earth. After less than three years of data taking, the statistical accuracy is insufficient to observe this effect, as visible in figure 16. The data slightly favors the presence of seasonal variation above 11.5 MeV in addition to the $\frac{1}{r^2}$ variation. More data is needed to observe a significant effect.

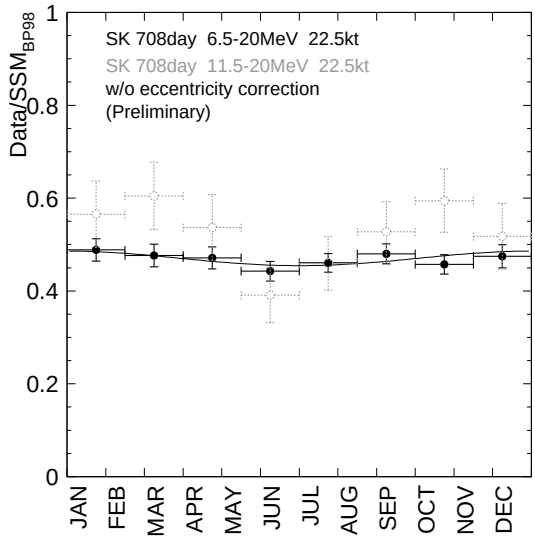

Fig. 16. Seasonal Variation The seasonal variation for the flux above 6.5 MeV (black filled in circles) and 11.5 MeV (grey open circles) shown is not corrected for the variation expected from spherical symmetry (black line).

6.6. Overall fit to the solar data

An overall fit to determine the neutrino parameters for MSW and vacuum oscillations (active and sterile neutrinos) that are allowed by the separate, and collective, imposition of the constraints from total event rates in the chlorine, GALLEX, SAGE, and SuperKamiokande experiments, the SuperKamiokande electron energy spectrum, and the SuperKamiokande zenith-angle dependence has been performed [21]. The small mixing angle MSW solution is acceptable at the 7% C.L. (8% for sterile ν's) and the vacuum

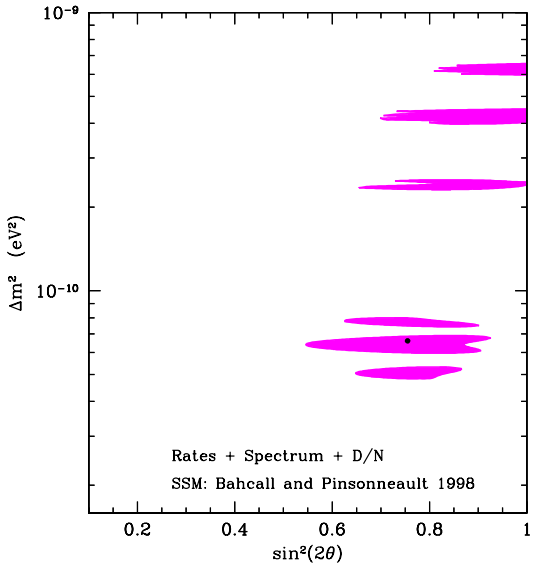

Fig. 17. Allowed parameter region [21] for vacuum oscillations that is consistent with the measured total rates, the recoil electron energy spectrum, and the Day-Night asymmetry. Contours are drawn at 99% C.L.

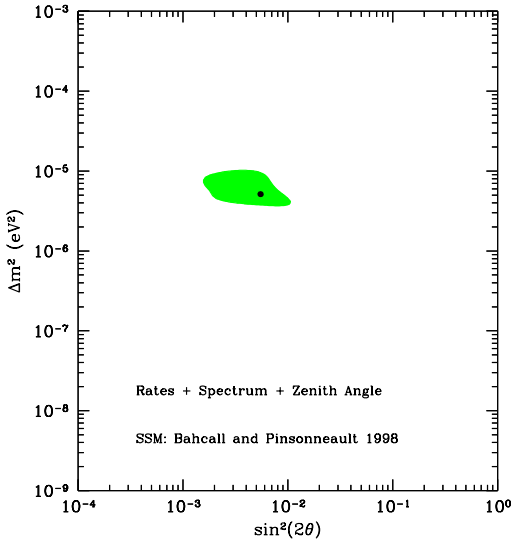

Fig. 18. Allowed region in MSW parameter space [21] that is consistent with the combined constraints from: the four measured rates, the SuperK electron recoil energy spectrum, and the SuperK zenith angle distribution.

solution is acceptable at the 6% C.L. For vacuum oscillations, the best-fit solution is: $\Delta m^2 = 6.5 \times 10^{-11}$ eV^2, $\sin^2(2\theta) = 0.75$. The allowed region is shown in figure 17. The best-fit global MSW solution for active neutrinos is: $\Delta m^2 = 5 \times 10^{-6}$ eV^2, $\sin^2(2\theta) = 5.5 \times 10^{-3}$ (and for sterile neutrinos: $\Delta m^2 = 4 \times 10^{-6}$ eV^2, $\sin^2(2\theta) = 7 \times 10^{-3}$). The allowed region is shown in figure 18. An arbitrary combination of undistorted (no oscillations) pp, 7Be, 8B, and CNO neutrino fluxes is shown to be inconsistent with the combined data sets at the 3.5 sigma C.L., independent of astrophysical considerations.

7. Atmospheric neutrinos

Experiments studying atmospheric neutrinos have up to now observed electrons and muons produced in charged current interactions and compared their observed numbers with the expected rates. At low energy (≈ 100 MeV up to a few GeV), the ratio of muon neutrino to electron neutrinos is $\simeq 2$, as both the primary pion produced in the atmosphere and their daugther muons decay before reaching the ground.

The absolute estimation of the rates is not an easy task and still suffers from quite large systematic uncertainties. The expected number of events is given by the product of the expected neutrino fluxes with the neutrino cross-sections:

$$N_{\ell^\pm}(E) \propto \phi_{\nu_\ell}(E) \times \sigma_{\nu_\ell}(E) + \phi_{\bar{\nu}_\ell}(E) \times \sigma_{\bar{\nu}_\ell}(E)\,,$$

where E is the neutrino energy. The neutrino fluxes have been calculated by various groups, the most recent published results are those of the Bartol group and by Honda *et al.* Both calculations agree reasonably well in the region of interest ($E_\nu \approx 200$ MeV up to about 100 GeV). An overall global uncertainty in the absolute flux of about 20% remains mostly due to the poor knowledge of the primary cosmic ray absolute flux. Geomagnetic fields of the Earth affect strongly the fluxes at low energy ($E < 1$ GeV) and are included in the calculations. Solar activity also influences the fluxes at low energy.

The neutrino cross-sections uncertainties are quite large in the low energy region of interest. Very few measurements of the cross-section have been performed at these low energies. They were performed in bubble chambers and where the data exists its statistical error is quite large. One could safely say that the uncertainty error in the cross-section is at the same level as that of the neutrino fluxes. The theoretical complication in correctly modelling the low energy neutrino cross-section comes from the treatment of the non-perturbative region (resonance region) and in the inclusion of proper nuclear effects since the target nucleon is not free.

Fortunately, lepton universality tells us that apart from small mass effects the cross-sections for electron and muon neutrino should be identical. Many uncertainties therefore cancel in the ratio

$$R = N_\mu / N_e.$$

This ratio reduces also most common uncertainties in the primary fluxes and is predicted with a 5% systematic uncertainty.

7.1. Anomalous ratio $RR = (N_\mu/N_e)_{\rm data}/(N_\mu/N_e)_{MC}$

Four early experiments — Kamiokande [24], IMB [25], NUSEX [26] and Frejus [27] — have published results on the double ratio of measured μ-like to e-like atmospheric events compared to that expected. The results are summarized in Table IX in which the exposure in $kt \times yr$ is also shown. The Kamiokande and IMB detectors using large water-Cerenkov detectors observed a ratio significantly less than expected, while Frejus and NUSEX both employing fine-grain iron-calorimeters find results strickingly consistent with expectations.

TABLE IX

Old and recent results from atmospheric neutrino experiments.

Experiment	Exposure (kt×yr)	$RR \equiv \frac{(\mu/e)_{\rm data}}{(\mu/e)_{\rm MC}}$
Kamiokande II/III multiGeV	8.2	$0.57^{+0.08}_{-0.07} \pm 0.07$
Kamiokande I/II/III subGeV	7.7	$0.60^{+0.06}_{-0.05} \pm 0.05$
IMB	7.7	$0.54^{\pm}0.05 \pm 0.11$
Frejus	2.0	$0.99 \pm 0.13 \pm 0.08$
NUSEX	0.74	1.04 ± 0.25
SuperKamiokande subGeV	45.5	$0.67 \pm 0.02 \pm 0.05$
SuperKamiokande multiGeV	45.5	$0.66 \pm 0.04 \pm 0.08$
Soudan-II	4.2	$0.66 \pm 0.11\ ^{+0.05}_{-0.06}$

The results of Kamiokande and IMB have been recently confirmed by the SuperKamiokande detector and by the Soudan-II measurements. The SuperKamiokande result dominates by its statistical accuracy. In fact, based on about 700 days of observation (or 45.5 kt × yr), the statistical accuracy is smaller than the systematic uncertainty.

The Soudan-II detector is a 1 kton fine-grained tracking calorimeter. While this experiment has the drawback of low statistics (exposure of 0.7 kt× yr/yr) compared to the SuperK experiment, it also observed an anomalous

ratio. Their latest result [28] for an exposure of 4.2 kt×yr is $0.66 \pm 0.11\ ^{+0.05}_{-0.06}$. Important aspects of their analysis have been checked by carrying out two independent, alternative analyses; one is based upon automated scanning, the other uses a multivariate approach for background subtraction. Similar results are found by all three approaches.

7.2. Zenith angle dependence

In atmospheric neutrino experiments, what has actually been measured is the energy of the final state lepton. At high energy, the direction of the produced charged lepton is strongly correlated with that of the incoming neutrino. In addition, the zenith angle of the incoming neutrino is a direct measure of the flight path L. For downward neutrino, the path length is about 10 km, while for upward going neutrinos which are produced below the horizon, the path length varies largely up to 12'000 km for neutrinos produced exactly on the other side of the Earth. Therefore, a zenith-angle dependent effect is a strong indication in favor of neutrino oscillation.

Kamiokande was the first to publish a zenith angle θ_z distribution of the double ratio RR that was apparently not in agreement with the expected shape. This distortion although not very statistically significant was interpreted as a possible hint for neutrino oscillations.

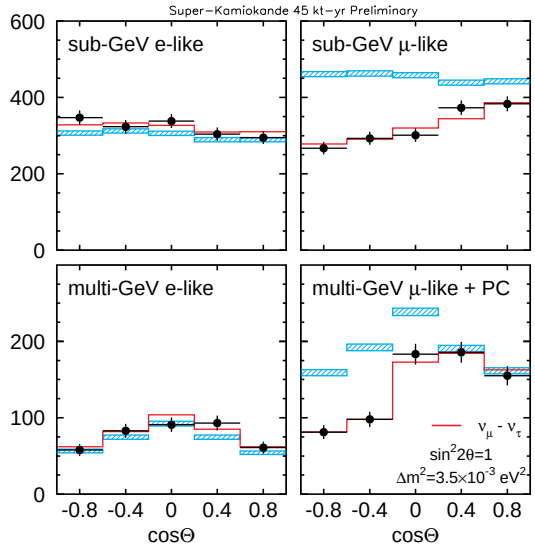

Fig. 19. Zenith angle θ_z distributions from events in SuperKamiokande. The best fitted oscillation parameters are $\Delta m^2 = 3.5 \times 10^{-3}$ eV^2 and maximal mixing. The fitted zenith angle distribution is shown (black full line).

The recent SuperKamiokande data has completely changed the situation. The zenith angle distributions for electron and muon samples are shown separately in figure 19. While the electrons seem to be in agreement with expectation, it is clear that there are less muon-like events in the upward direction than expected while in the downward direction they are consistent with expectation.

Soudan-II has in addition the capability to observe the recoil proton in the neutrino interaction. This substantially improves the resolution on θ_z, the angle of the incoming neutrino. Somewhat surprisingly, the Soudan-II high resolution muon sample does not exhibit a large up/down asymetry as observed in SuperKamiokande. Instead, there clearly appears to be a muon deficit essentially independent of the zenith angle. This forces the fitted Δm^2 to lie above 1.2×10^{-3} eV^2.

7.3. Upward going muons

Neutrinos will travel through the earth. Upward-going muons are produced by high-energy atmospheric neutrinos which interact in the rock around the detector. Those which pass completely through the detector have a mean parent neutrino energy of ≈ 100 GeV, while those which range out inside the detector come from neutrinos of mean energy ≈ 10 GeV. The neutrino baseline varies with the observed muon zenith angle, allowing for an independent test via ν_μ disappearance of the neutrino oscillations observed in events where the neutrino interacted in the detector. In this case, a ratio to ν_e events cannot be used to reduce sensitivity to uncertainties in the ν_μ flux. However, comparisons are made to a wide range for flux models.

SuperKamiokande has observed 614 upward through-going and 137 upward stopping muons over 537 (516) live days [32]. The observed stopping over through-going ratio $R = 0.218 \pm 0.023(\text{stat.})^{+0.014}_{-0.013}(\text{syst.})$ is 2.9 sigma lower than the expectation. Both the shape of the zenith angle distribution of the observed flux and this low ratio are inconsistent with the null oscillation hypothesis, but are compatible with the previously observed oscillation hints. Taken as a whole, the addition of these higher energy ν_μ data to the contained neutrino events provides a better measurement of the oscillation parameters, narrowing the allowed parameter range to $\sin^2 2\theta > 0.9$ and 1.5×10^{-3} eV$^2 < \Delta \text{m}^2 < 6 \times 10^{-3}$ at 90% confidence (see next section).

MACRO [29] has performed a measurement of the flux of neutrino-induced muons. Different event topologies, corresponding to different neutrino parent energies can be detected. The upward through-going muon sample is the larger event sample. The observed upward-through-going muons are 26% fewer than expected and the zenith angle distribution does not fit with the expected one. The ratio is $0.74 \pm 0.036(\text{stat.}) \pm 0.046(\text{syst.}) \pm 0.013(\text{th})$, which includes the systematic error on the flux calculation. As-

suming neutrino oscillations, both measurements suggest maximum mixing and a Δm^2 of a few times 10^{-3} eV^2. The other samples are due to the internally produced events and to upward-going stopping muons. These data show a regular deficit of observed events in each angular bin, as expected assuming neutrino oscillations with maximum mixing, in agreement with the analysis of the upward-throughgoing muon sample.

7.4. Evidence for neutrino oscillations

SuperKamiokande based on their large statistical accuracy and complete systematic checks have published recently an "evidence for neutrino oscillations" [30]. There are now three effects in favor of an interpretation of the atmopheric neutrino anomaly in terms of flavor oscillations:

- the anomalous ratio of neutrino events
- the zenith angle distribution
- the zenith angle distribution of upward through-going muons.

SuperKamiokande has made a quantitative global fit of the subGeV and multiGeV data assuming oscillations. The global χ^2 analysis suggests the following:

- no neutrino oscillations: $\chi^2_{\rm min} = 175/69$ dof!
- $\nu_\mu \to \nu_e$ oscillations: $\chi^2_{\rm min} = 110/67$ dof with oscillation parameters $\sin^2 2\theta = 0.98$ and $\Delta m^2 = 3.8 \times 10^{-3}$ eV^2.
- $\nu_\mu \to \nu_\tau$ oscillations: $\chi^2_{\rm min} = 61.5/67$ dof with oscillation parameters $\sin^2 2\theta = 1.05$ and $\Delta m^2 = 2.9 \times 10^{-3}$ eV^2. Constraining $\sin^2 2\theta = 1$ yields $\chi^2_{\rm min} = 62.1/66$ dof and $\Delta m^2 = 3.5 \times 10^{-3}$ eV^2

The no-oscillation hypothesis is ruled out! The oscillation into electron is disfavoured and is excluded also by the CHOOZ [31] result. The conversion into tau neutrino provides a very good fit to the data. Figure 20 shows the allowed region in the $(\sin^2 2\theta, \Delta m^2)$ plane for $\nu_\mu \to \nu_\tau$ oscillations.

In addition, SuperKamiokande has also combined their upward going muon data to further constrain the oscillation parameters. The results are:

- no neutrino oscillations: $\chi^2_{\rm min} = 214.3/85$ dof!
- $\nu_\mu \to \nu_\tau$ oscillations: $\chi^2_{\rm min} = 69.4/82$ dof with oscillation parameters $\sin^2 2\theta = 1.05$ and $\Delta m^2 = 3.2 \times 10^{-3}$ eV^2. Constraining $\sin^2 2\theta = 1$ yields $\chi^2_{\rm min} = 70.2/81$ dof and $\Delta m^2 = 3.2 \times 10^{-3}$ eV^2

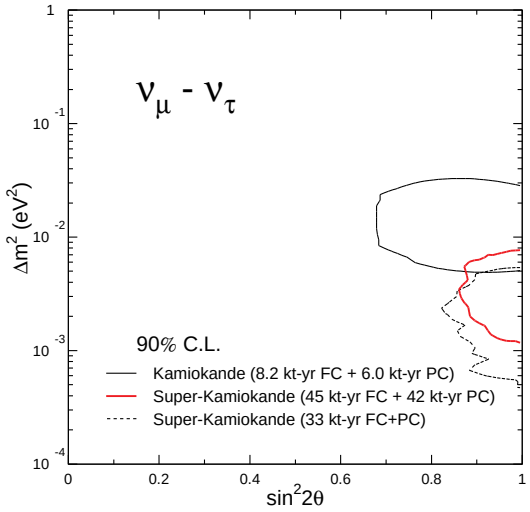

Fig. 20. Allowed region of the oscillation parameter space as fitted by SuperKamiokande SubGeV and MultiGeV sample. The old result from Kamiokande is also shown.

7.5. Determination of the oscillation parameters

The atmospheric neutrino anomaly is seen by various experiments and by various analysis methods. Table X summarizes Δm^2 for the hypothesis that the atmospheric neutrino deficit is entirely explained by $\nu_\mu \to \nu_\tau$ oscillations. All results are consistent with this oscillation hypothesis. Experiments quote either a "best fit" or a "consistent" Δm^2 value, as noted.

TABLE X

Δm^2 from $\cos\theta_z$ dependence of atmospheric neutrino experiments using the $\nu_\mu \to \nu_\tau$ oscillation hypothesis. Results that do not have a "best fit" quoted by the experiment are listed with the Δm^2 which is described as "consistent with" the data.

Experiment	Analysis	Δm^2 is ...	Δm^2(eV)^2
Kamiokande	R	best fit	1.6×10^{-2}
Kamiokande	up-going μ	best fit	3.2×10^{-2}
Super K	R	best fit	2.2×10^{-3}
Super K	up-going μ	consistent with	2.5×10^{-3}
Soudan II	R	consistent with	$> 10^{-3}$
MACRO	up-going ν	consistent with	5×10^{-3}
MACRO	up-going μ	consistent with	2.5×10^{-3}

8. Future tests of the atmospheric anomaly

8.1. ICARUS T600 detector

ICARUS [11, 12] is an approved experiment of the Gran Sasso National Laboratory with the main goals of searching for proton decay and of studying atmospheric and solar neutrinos. The realization of a 600 ton liquid argon (LAr) TPC represents the first step of the ICARUS project. It will be shielded from most cosmic rays by placing it underground in the GranSasso National Laboratory near Rome, Italy.

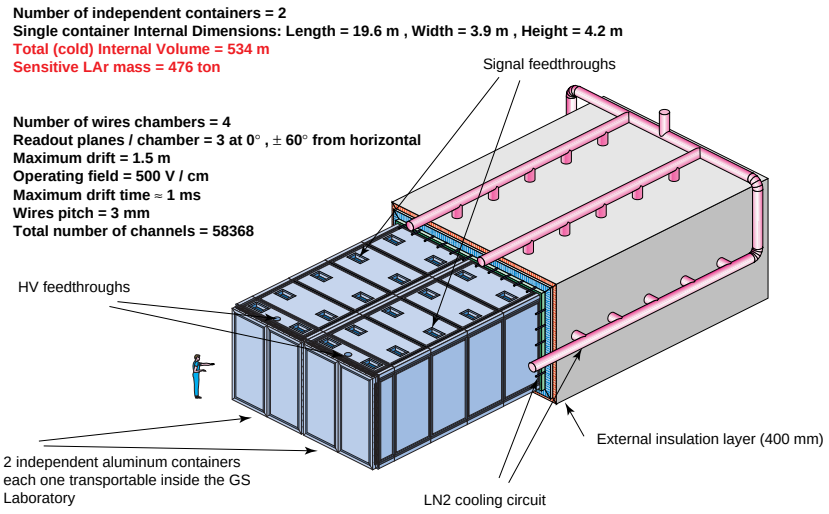

Fig. 21. A 3-dimensional sketch of the ICARUS T600 cryostat. The detector will be located in the Gran Sasso National Laboratory (LNGS, Italy) in order to study cosmic rays and solar neutrinos and search for proton decay.

ICARUS provides an excellent general purpose large scale neutrino detector: it offers within the same volume a tracker in three dimensions with high spatial resolution and particle identification, and also, because of the high density of the liquid medium, precise homogeneous calorimetry. A neutrino event detected with a small prototype (50 litres) of the ICARUS detector is shown in figure 22. The main characteristics of ICARUS are the following:

— It is a homogeneous tracking device, capable of dE/dx measurement. The high dE/dx resolution allows both good momentum measurement and particle identification for soft particles.

— Electromagnetic and hadronic showers are fully sampled. This allows to have a good energy resolution for both electromagnetic, $\sigma(E)/E \simeq$

Fig. 22. An example of recorded neutrino interaction in a 50 liter Liquid Argon TPC prototype exposed at the CERN ν beam. The neutrino comes from the top of the picture. The horizontal axis is the time axis (drift direction) and vertically is the wire number. The visible area corresponds to 47×32 cm^2

$3\%/\sqrt{E/\mathrm{GeV}}$, and hadronic contained showers, $\sigma(E)/E \simeq 15\%/\sqrt{E/\mathrm{GeV}}$.

— It has good electron identification and e/π^0 discrimination thanks to the ability to distinguish single and double m.i.p. by ionization and to the bubble chamber quality space resolution.

During 1998, the main activities were related to the construction of the 600 ton module (see figure 21). The design of the cryostat and of its components has continously evolved and the first half-module is presently being assembled. Its delivery is foreseen before the summer of 1999.

A 10m^3 prototype cryostat has also been built and prepared for a series of complete tests which have started in the beginning of 1999. This 15 ton detector serves as a test bench for the 600 ton detector. In particular, the cryogenic system and control will be identical as the one for the 600 ton. The 15 ton is also used to test the internal detector and the associated cryogenic instrumentation.

9. The long baseline programmes

9.1. K2K

TABLE XI

List of relevant parameters for the present CERN neutrino beam and for the anticipated beams at KEK, at Fermilab and at CERN. The CERN NGS figures correspond to a "shared" mode of operation. More intensity could be achieved in a dedicated mode.

	CERN WANF	K2K	FNAL NUMI	CERN NGS
Protons:				
Energy (GeV)	450	12	120	350-450
Pot/cycle	2×10^{13}	6×10^{12}	4×10^{13}	9×10^{13}
Cycle time (s)	14.4	2	1.9	26.4
Days/year	200×0.75	250×0.7	300×0.67	200×0.75
Pot/year	1.5×10^{19}	4.5×10^{19}	3.7×10^{20}	4.5×10^{19}
Long-baseline ν's:				
$< E(\nu_{\mu CC}) >$	—	1.5 GeV	16 GeV	17 GeV
ν_μ CC/kt/10^{19}	—	2	100	600
ν_μ CC/year	—	$\approx$ 200/22.5kt	$\approx$ 3800/kt	2700/kt
ν_τ appearance	—	No	Yes/No	Yes
Status:				
Running date	$\rightarrow$ 1998	1999 $\rightarrow$	2002 $\rightarrow$	2004(?) $\rightarrow$

The first long baseline accelerator experiment (see Table XI) to address the atmospheric anomaly will use a neutrino beam from the KEK 12 GeV proton synchrotron in conjunction with the SuperKamiokande detector at a distance of 250 km. The **K2K** [33] program is currently under construction in Japan. This experiment should start data taking in 1999. Both ν_μ disappearance and ν_e appearance will be studied. However, because of a low energy beam $E_\nu \approx 1.4$ GeV, it will not be possible to study the tau appearance directly, hence, the $\nu_\mu \rightarrow \nu_\tau$ hypothesis will have to be inferred from a comparison of the $\nu_\mu \rightarrow \nu_e$ appearance and $\nu_\mu \rightarrow \nu_x$ disappearance rates resulting in poor mixing sensitivity.

9.2. FNAL/NUMI and CERN/NGS

The future neutrino program at Fermilab includes a long base-line experiment. The neutrino beam from the Main Injector is directed towards the Soudan underground laboratory in Minnesota at a distance of 730 km from Fermilab.

A possibility that would take advantage of the already approved program in the underground laboratory at the Gran Sasso National Laboratory, which consists in aiming a neutrino beam from the CERN SPS to Gran Sasso at a distance of 732 km, has been discussed for many years [12].

As for the beam, the general strategy was to opt for a wide band neutrino beam based on the experience gathered at CERN with the design and the operation of the WANF. The beam optimization and the design of the details of the beam optics have been subject of further studies driven by the requests of the experiments. Following the indication of the CERN–LNGS committee, a first optimization of the beam has been carried out with the goal of maximizing the ν_τ CC interactions at LNGS for appearance experiments.

Options of lower energy beam have also been considered for disappearance experiments. Further studies on the optimisation of the beam are currently being done.

9.3. Long baseline detectors

The proposed detector at FNAL, **MINOS** [34], is based on 5 ktons of magnetized iron plates interspaced by scintillators, to be installed in the Soudan mine. Various methods have been discussed in the proposal in order to extract possible oscillation signals. With such a coarse detector, the best sensitivity will probably be reached by studying the "event without muon" over "event with muon" ratio. Unless an extra emulsion target is placed in the front of the detector, this experiment will be limited to perform disappearance studies.

TABLE XII

Expected number of atmospheric neutrino interactions for an exposure of 30 kton x year and E_{ν_μ} down to threshold, E_{ν_e} down to 50 MeV.

	C. C.	N.C.	C.C. + N. C.
ν_μ	3432	1301	4733
ν_e	1800	659	2459
$\bar{\nu_\mu}$	876	493	1369
$\bar{\nu_e}$	414	250	664
$\nu_\mu + \bar{\nu_\mu}$	4308	1794	6102
$\nu_e + \bar{\nu_e}$	2214	909	3123
all events	6522	2703	9225

At the CERN/NGS, there have been numerous proposals. The most interesting aspect is the possibility to detect ν_τ CC interactions, an ultimate proof of flavor oscillation. Based on the NOMAD and CHORUS expertise developed at CERN during the 80's, detectors capable of detecting the presence of tau lepton in the event final states have been proposed. The detectors are described below. Table XIII summarizes the number of tau CC events fully reconstructed that would be observed in the various exper-

TABLE XIII

Tau appearance at the CERN-NGS. The number of background and detected tau events as a function of Δm^2 for 4 years of running (shared-more) at the CERN-NGS.

Exp.	Background	Number of detected tau events, Δm^2 eV^2			
		2×10^{-3}	3.5×10^{-3}	5×10^{-3}	10^{-2}
ICARUS 2.4kt	2.5	13	40	85	340
SuperICARUS	3.7	70	200	420	1700
OPERA	0.4	6	20	40	150
NOE 8kton	3.7	2	7	15	60

iments after 4 years of running in a "shared" SPS mode, compared to small backgrounds. The experiments proposed at the NGS have the potentiality to unambiguously prove the flavor oscillation.

ICARUS [11, 12] Because of the high resolution on measuring kinematical quantities, the ν_τ appearance search in ICARUS is based on the kinematical suppression of the background using similar techniques to those of the NOMAD experiment [2].

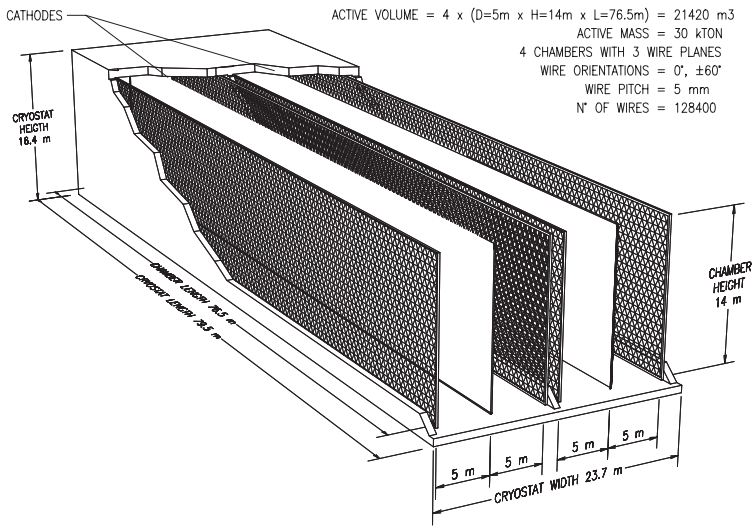

Fig. 23. A 3-dimensional sketch of the proposed SuperICARUS detector.

Recently the possibility to build a **SuperICARUS** detector of 30 kt (see figure 23) has been put forward [35]. One of the aims of this detector would be to increase the sensitivity to neutrino oscillations at low mixing and in

the low Δm^2 region. SuperICARUS would allow the collection of about 9200 atmospheric neutrinos per year (see Table XII), fully reconstructed with good precision. These are largely sufficient to elucidate the presence of oscillations in the cosmic rays. In presence of the neutrino oscillation, charged current ν_τ events will appear in atmospheric neutrino events. This will offer the possibility of a ν_τ appearance experiment in the cosmic ray events, independently from the searches with the beam. An exposure of 4 effective years at $\Delta m^2 = 3.5 \times 10^{-3}$ eV^2 would lead to about 120 tau events before cuts. The possibility to detect these events with a $S/N \approx 1$ has been demonstrated in Ref. [36].

OPERA [37] is a conceptual design of a massive detector able to operate on a medium or long baseline location, to explore $\nu_\mu - \nu_\tau$ oscillations based on the emulsion technique. In OPERA, emulsions are used as high precision trackers, unlike in CHORUS where they compose the active target. The extremely high space resolution of the emulsion should cope with the peculiar signature of the short lived τ lepton, produced in the interactions of the ν_τ.

The OPERA detector consists of a 0.75 kt lead emulsion target. The basic element (*cell*) of the detector is composed of a 1mm thick lead-plate followed by an emulsion sheet (ES1), a 3mm drift space (filled with low density material) and another emulsion sheet (ES2) (see figure 24). An ES1(ES2) is made of a pair of emulsion layers 50 micron thick, on either side of a 100(200) micron plastic base. Thirty cells are arranged together to form a *brick*, which has $15 \times 15 \times 13\text{cm}^3$ dimensions; bricks are put together to form a *module* ($2.8 \times 2.8 \times 0.15\text{m}^3$).

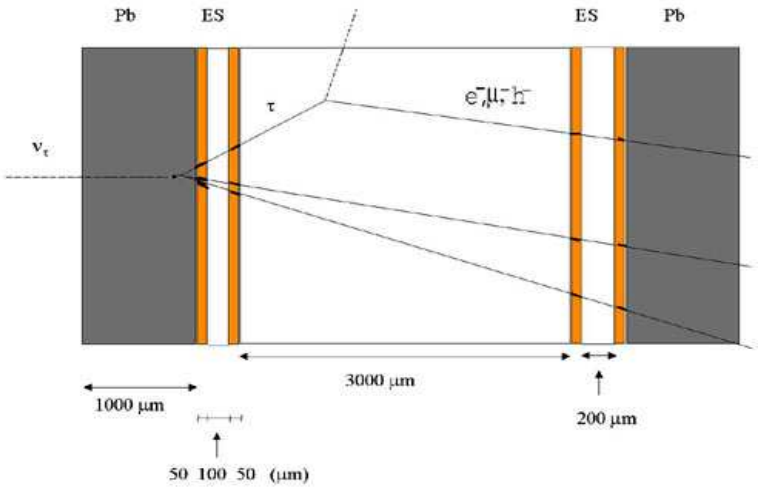

Fig. 24. The basic elements of the OPERA detector.

Since the emulsion does not have time resolution, there are electronic detectors after each module in order to correlate the neutrino interactions to the brick where they occur and to guide the scanning. Streamer tubes have been proposed as electronic detectors, but other possible solutions are under study. A total of 300 modules are subdivided into 10 identical *super-modules*. The overall dimensions of the detector are $3.5 \times 3.5 \times 40\text{m}^3$.

The τ's produced in ν_τ CC interactions, are detected by measuring their decay kink when occurring in the drift space. The kink angle is measured by associating two high-precision 3-D track segments reconstructed in ES1 and ES2. The present estimate of the OPERA τ detection efficiency is about 35%. We observe that the τ decays in the lead-target plates are not lost, but they do not offer the same golden background conditions. Studies are under way in order to use them to further increase the overall detection efficiency.

The main source of background for the decays inside the gap is the production of charged charm particles with subsequent decay when the primary lepton is not detected. Monte Carlo simulation showed that the number of background events expected from this source is below 1 in four years. Thus OPERA is believed to be essentially free of backgrounds.

NOE [38] has been proposed as a long baseline experiment to study $\nu_\mu \to \nu_\tau$ and $\nu_\mu \to \nu_e$ oscillations. The basic elements of the NOE detector are *light* transition radiation detector modules (TRD) for a total TRD mass of 2.4kt interleaved with modules of a massive fine grain $5.6kt$ calorimeter (CAL). A TRD and a CAL module together form the basic module of the NOE detector. The whole $8kt$ NOE detector is made of 12 subsequent basic modules.

Combining both CAL and TRD information, the rejection power to separate electrons from minimum ionising particles is $10^{-3} - 10^{-4}$. The e/π^0 discrimination is based on the fact that, because of the light TRD material, π^0's cross many TRD layers with low conversion probability.

The $\nu_\mu \to \nu_\tau$ oscillation search is performed by kinematical identification of the τ lepton decays, exploiting the techniques developed by the NOMAD collaboration [2]. So far the $\tau \to e$ channel has been fully studied. The possibility to use the $\tau \to \pi$ channels is encouraging.

10. New generation of neutrino beams

In the last few years there has been growing interest in studying the technical feasibility and the impact on physics of a muon collider with high intensity beams. These machines are attractive for new generation neutrino beams [39]. Indeed,

- The very large protons intensities in the range of 10^{22} protons/year needed for the muon collider opens up new domain of neutrino fluxes in which secondary hadrons are producing an intense neutrino beam;

- Muons decaying in this collider are a continuous source of both muon and electron-like neutrinos via the following relation: $\mu^{\pm} \to e^{\pm}\nu_e\nu_\mu$.

The muons are produced in the decay chain of pions behind an appropriate target and are subsequently captured, cooled, accelerated and stored into a ring where they are let to decay. The total number of muons accelerated is computed in the following way:

$$N_\mu = f_{\text{bunch}} \times N_{p/\text{bunch}} \times Y_{\pi/p} \times Y_{\mu/\pi} \times t\,,$$

where f_{bunch} is the bunch repetition rate, $N_{p/\text{bunch}}$ is the number of protons per bunch, $Y_{\pi/p}$ is the yield of pions per proton, and $Y_{\mu/\pi}$ is the yield of muons per pion. It is assumed that $Y_{\pi/p} \times Y_{\mu/\pi} = 0.08$ muons per proton will be trapped and accelerated into the storage ring.

When a neutrino beam is produced from muons of a definite sign, only one kind of flavor-antiflavor is produced.

In case of $\nu_\mu \to \nu_e$ oscillations, there will be appearance of ν_e neutrinos while the unoscillated beam contained only $\bar{\nu}_e$'s. Charge discrimination in the detector will trivially separate the two types of neutrino components:

$$\bar{\nu}_e + N \;\to\; e^+ + X \qquad \text{intrinsic beam component,} \tag{21}$$

$$\nu_e + N \;\to\; e^- + X \qquad \text{oscillated} \tag{22}$$

In case of $\bar{\nu}_e \to \bar{\nu}_\mu$ oscillations, there will be appearance of $\bar{\nu}_\mu$ neutrinos while the unoscillated beam contained only ν_μ's.

$$\nu_\mu + N \;\to\; \mu^- + X \qquad \text{intrinsic beam component,} \tag{23}$$

$$\bar{\nu}_\mu + N \;\to\; \mu^+ + X \qquad \text{oscillated} \tag{24}$$

Such an experiment could test the transition $\nu_\mu \to \nu_e$ and its CP-conjugate $\bar{\nu}_\mu \to \bar{\nu}_e$ at the same time.

10.1. Testing the LSND result

In Ref. [14], it was pointed out that the currently existing CERN-PS machine, able to accelerate $f_{\text{bunch}} \times N_{p/\text{bunch}} \times t \approx 2.5 \times 10^{20}$ protons in a year at an energy of 19.2 GeV, could be used as a proton driver. Under this assumption, the total number of muons accelerated is $2 \times 10^{19}\mu$/year. After 2 years of running, a total of $4 \times 10^{19}\mu$ will have decayed inside the storage ring.

A medium baseline from the CERN-PS to the CERN-Prevessin laboratory, close to the North Area, was chosen in order to test the LSND signal.

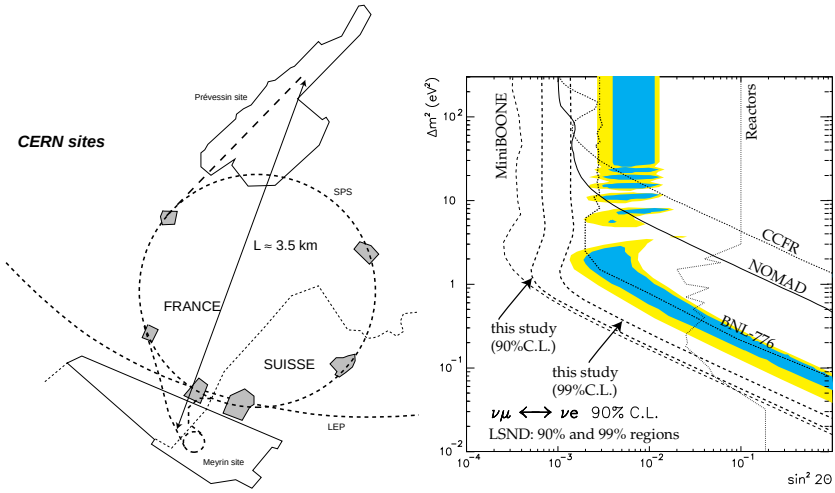

Fig. 25. (a) Schematic overview of the CERN sites. (b) Predicted negative limits at the 90% C.L. and 99% C.L. for the study [14] compared to expected MiniBOONE 90% C.L. limit for neutrino oscillation appearance. Negative results from previous NOMAD, CCFR, BNL-776 and reactor experiments are also shown.

The distance from the PS is about 3.5 km (see figure 25) and therefore the "modest" proton intensity (while inadequate for a muon collider) would allow to test the technology of neutrino beams from muon decays. The existing NOMAD detector was tentatively used as a target. The muon beam energy was set to 7 GeV in order to obtain a relatively low energy neutrino beam. In case of negative result, combining both channels assuming CP conservation, the 90% C.L. limit on $\nu_\mu \to \nu_e$ oscillations, for a total flux of 4×10^{19} muons, corresponds to a limit on the mixing angle for large Δm^2 of

$$\sin^2 2\theta < 7 \times 10^{-4} \qquad 90\% \text{ C.L.} \tag{25}$$

and $\Delta m^2 > 2 \times 10^{-2}$ eV^2 for maximal mixing. The 90% and 99% C.L. exclusion contours are shown in figure 25b compared to the LSND positive solution, the current limits from NOMAD, CCFR and reactor experiments, and the expected limit from MiniBOONE. The LSND solution is well covered by the sensitivity obtained.

11. Conclusions

The inclusion of neutrino masses and mixings is nowadays considered as a natural "extension" of the Standard Model. The exact format of this extension is however not yet defined, since the neutrality of the neutrino allows for more complicated mass terms than for charged fermions. This

natural extension of the Standard Model is motivated by the accumulation of experimental effects that are well explained in terms of neutrino flavor oscillations. While the searches for $\nu_\mu \to \nu_\tau$ oscillations at high Δm^2 and small mixings have led negative results, the results from SuperKamiokande are now interpreted as "evidence" for flavor oscillations, most likely between maximally mixed ν_μ and ν_τ. The mostly favored explanation of the solar neutrino deficit is clearly via neutrino oscillated induced disappearance of ν_e's. New experiments looking specifically for "smoking guns" will be needed to really clarify the situation. The LSND signal, indicating much higher mass differences than either atmospheric and solar neutrinos, fails to be confirm nor disproved. It currently remains hanging and new generation experiments will be needed to settle the debate. These continue to be exciting times for neutrino physics!

I thank the organizers of the workshop for inviting me, in particular, F. del Aguila. I thank A. Bueno for his numerous careful readings of the manuscript.

REFERENCES

[1] B. Pontecorvo, *Zh. Eksp. Teor. Fiz.* **53**, 1717 (1967); *Zh. Eksp. Teor. Fiz.* **34**, 247 (1958); *Zh. Eksp. Teor. Fiz.* **33**, 549 (1957). B. Kayser, *Phys. Rev.* **D24**, 110 (1981).

[2] NOMAD Collaboration (P. Astier *et al.*). CERN-EP-99-032, Feb 1999. J. Altegoer *et al.* [NOMAD Collaboration], *Phys. Lett.* **B431**, 219 (1998).

[3] CHORUS Collab., E. Eskut *et al.*, *Phys. Lett.* **B434**, 205 (1998). CHORUS Collab., E. Eskut *et al.*, *Phys. Lett.* **B424**, 202 (1998).

[4] N. Ushida *et al.*, (E531 Collab.), *Phys. Rev. Lett.* **57**, 2897 (1986).

[5] C. Athanassopoulos *et al.*, (LSND Collaboration), *Phys. Rev.* **C54**, 2685 (1996); C. Athanassopoulos *et al.*(LSND Collaboration), *Phys. Rev. Lett.* **77**, 3082 (1996); *Phys. Rev. Lett.* **75**, 2650 (1995). Updated results including 1997 data can be found at `http://www.neutrino.lanl.gov/LSND/papers.html`.

[6] C. Athanassopoulos *et al.* [LSND Collaboration], *Phys. Rev. Lett.* **81**, 1774 (1998); C. Athanassopoulos *et al.* [LSND Collaboration], "Evidence for muon-neutrino → electron-neutrino oscillations from pion decay in flight neutrinos", nucl-ex/9706006.

[7] K. Eitel *et al.* [KARMEN Collaboration], "The Search for neutrino oscillations muon anti-neutrino → electron anti-neutrino with KARMEN", hep-ex/9809007.

[8] G.J. Feldman, R.D. Cousins, "Unified approach to the classical statistical analysis of small signals", *Phys. Rev.* **D57**, 3873 (1998).

[9] E. Church *et al.*, "A proposal for an experiment to measure muon-neutrino → electron- neutrino oscillations and muon-neutrino disappearance at the Fermilab Booster: BooNE", FERMILAB-P-0898. Updated information on the BOONE proposal can be found at *http://www.neutrino.lanl.gov/BooNE/*.

[10] F. Vannucci *et al.*, CERN SPSLC/P178 (SPSLC 82-20), March 1982, unpublished.

[11] ICARUS-CERN-Milano Coll., CERN/SPSLC 96-58, SPSLC/P 304, December 1996; J. P. Revol *et al.*, ICARUS-TM-97/01, 5 March 1997, unpublished.

[12] ICARUS Collaboration, Laboratori Nazionali del Gran Sasso (LNGS) Int. Note, LNGS - 94/99 (Vols I-II), unpublished; LNGS 95/10, unpublished. P. Benetti *et al.*, *Nucl. Instrum. Methods* **A327**, 173 (1993);*Nucl. Instrum. Methods* **A332**, 395 (1993); P. Cennini *et al.*, *Nucl. Instrum. Methods* **A333**, 567 (1993);*Nucl. Instrum. Methods* **A345**, 230 (1994); *Nucl. Instrum. Methods* **A355**, 660 (1995).

[13] N. Armenise *et al.*, CERN-SPSC/97-21, October 1997.

[14] A. Bueno, M. Campanelli, A. Rubbia, "A Medium baseline search for neutrino(mu) → neutrino(e) oscillations at a neutrino beam from muon decays," hep-ph/9809252 and CERN-EP-98-140.

[15] A. Bueno, M. Campanelli, A. Rubbia, "Long baseline neutrino oscillation disappearance search using a neutrino beam from muon decays," hep-ph/9808485 and ETHZ-IPP-PR-98-05.

[16] J.N. Bahcall, S. Basu, M.H. Pinsonneault, Phys. Lett. **B433**, 1 (1998) and references therein. J.N. Bahcall, M.H.Pinsonneault, *Rev. Mod. Phys.* **67**, 781 (1995). Updated information can be found at *http://www.sns.ias.edu/$\tilde{}$jnb/*.

[17] R. Davis, (Homestake Collab.), *Prog. Part. Nucl. Phys.* **32**, 13 (1994); B. T. Cleveland *et al.*, (Homestake Collab.), *Nucl. Phys. B (Proc. Suppl.)* **38**, 47 (1995).

[18] K.S. Hirata *et al.*, *Phys. Rev. Lett.* **65**, 1297 (1990); *Phys. Rev. Lett.* **65**, 1301 (1990); *Phys. Rev. Lett.* **66**, 9 (1991); *Phys. Rev.* **D44**, 1991 (1991).

[19] J. N. Abdurashitov *et al.*(SAGE Collab.), *Phys. Rev. Lett.* **77**, 4708 (1996). W. Hampel *et al.*(GALLEX Collab.), *Phys. Lett.* **B388**, 384 (1996)

[20] J.N. Bahcall, R.K. Ulrich, Rev. Mod. Phys. **60**, 297 (1988).

[21] J.N. Bahcall, P.I. Krastev, A.Y. Smirnov, Phys. Rev. **D58**, 096016 (1998) hep-ph/9807216.

[22] L. Wolfenstein, *Phys. Rev.* **D17**, 2369 (1978); *Phys. Rev.* **D20**, 2634 (1979); S.P. Mikeyev, A.Yu. Smirnov, *Nuovo Cim.* **9C**, 17 (1986).

[23] J.N. Bahcall, P.I. Krastev, Phys. Lett. **B436**, 243 (1998) hep-ph/9807525.

[24] K.S. Hirata *et al.*, *Phys. Lett.* **B205**, 416 (1988); *Phys. Lett.* **B280**, 146 (1992); Y. Fukuda *et al.*, *Phys. Lett.* **B335**, 237 (1994).

[25] R. Becker-Szendy *et al.*, (IMB Collab.), *Phys. Rev.* **D46**, 3720 (1992).

[26] M. Aglietta *et al.*, (NUSEX Collaboration), Europhys. Lett. **8**, 611 (1989).

[27] Ch. Berger *et al.*, (Fréjus Collaboration), *Phys. Lett.* **B245**, 305 (1990).

[28] W.W. Allison *et al.* [Soudan-2 Collaboration], Phys. Lett. **B449**, 137 (1999) hep-ex/9901024.

[29] F. Ronga *et al.* [MACRO Collaboration], "Atmospheric neutrino induced muons in the MACRO detector," hep-ex/9810008.

[30] Y. Fukuda *et al.* [SuperKamiokande Collaboration], Phys. Rev. Lett. **81**, 1562 (1998), hep-ex/9807003.

[31] M. Apollonio *et al.* [CHOOZ Collaboration], Phys. Lett. **B420**, 397 (1998), hep-ex/9711002.

[32] A. Habig [SuperKamiokande Collaboration], "Neutrino induced upward going muons in SuperKamiokande," hep-ex/9903047.

[33] M. Sakuda [K2K Collaboration], "The KEK-PS long baseline neutrino oscillation: Experiment (E362)," *Submitted to APCTP Workshop: Pacific Particle Physics Phenomenology (P4 97), Seoul, Korea, 31 Oct - 2 Nov 1997.*

[34] E. Ables *et al.* [MINOS Collaboration], "P-875: A Long baseline neutrino oscillation experiment at Fermilab," FERMILAB-PROPOSAL-P-875.

[35] The ICARUS collaboration, *ICARUS-Like Technology for Long Baseline Neutrino Oscillaitons*, CERN/SPSC/98-33 & M620, 1998.

[36] A. Bueno, A. Rubbia, "Detecting the presence of ν_τ in the atmospheric neutrino flux", ICARUS/TM-99/11, April 1999.

[37] A. Ereditato, K. Niwa, P. Strolin, INFN/AE-97/06 and Nagoya DPNU-97-07, 27 January 1997, unpublished.

[38] M. Ambrosio *et al.*, LNGS/Note 94-112 (1994), unpublished; G.Barbarino *et al.*,*Nucl. Phys.* **B48**, 204 (1996).

[39] S.Geer, *Phys. Rev.* **D57**, 6989 (1998).